# Theoretical Studies of Oxidative Addition and Reductive Elimination. 2. Reductive Coupling of H–H, H–C, and C–C Bonds from Palladium and Platinum Complexes[†]
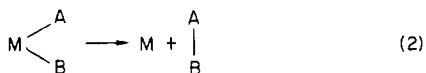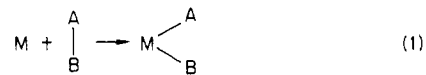
John J. Low[‡] and William A. Goddard, III[*]

Arthur Amos Noyes Laboratory of Chemical Physics, California Institute of Technology, Pasadena, California 91125

Received February 25, 1985

Ab initio calculations have been carried out on $MR_2$ complexes (where M = Pd or Pt and R = H or $CH_3$) to model concerted reductive coupling from $MR_2L_2$ complexes (where L is a substituted phosphine). The results of these calculations support the following two conclusions. (1) The difference in the driving force for reductive elimination from Pd(II) and Pt(II) complexes with the same R groups is very close (0–4 kcal/mol) to the difference in the $s^1d^9$–$d^{10}$ state splittings of these elements (32 kcal/mol). Thus reductive elimination is exothermic from Pd complexes (since Pd prefers $d^{10}$) and endothermic from Pt complexes (since Pt prefers $s^1d^9$), where the metal product is in its $d^{10}$ state. This supports the conclusion, derived from qualitative considerations of generalized valence bond wave functions, that Pt(II) and Pd(II) complexes have their metal atoms in an $s^1d^9$ configuration and the metal atoms in Pt(0) and Pd(0) complexes are in a $d^{10}$ configuration. (2) The activation barriers for C–C coupling are approximately twice that for C–H coupling. There are essentially no barriers for processes involving H–H bonds. The origin of this trend is the directionality of the methyl $sp^3$ orbital, which destabilizes the transition state for the case where an M–C bond is being converted to a C–C or C–H bond. Conversely, the spherical H 1s orbital can form multicenter bonds easily, allowing it to break M–H bonds while forming an H–H bond and leading to low intrinsic barriers. These results are consistent with the experimentally observed trends.

## I. Introduction

The concepts of oxidative addition (eq 1) and reductive elimination (eq 2) are prevalent in the literature on organometallic chemistry.[1] Thus, catalytic hydrogenation

$$M + \begin{matrix} A \\ | \\ B \end{matrix} \longrightarrow M \begin{matrix} A \\ \diagup \\ \diagdown \\ B \end{matrix} \qquad (1)$$

$$M \begin{matrix} \diagup A \\ \diagdown B \end{matrix} \longrightarrow M + \begin{matrix} A \\ | \\ B \end{matrix} \qquad (2)$$

of alkenes often requires oxidative addition of $H_2$ to form the activated complex $MH_2$;[2] e.g., eq 3 involves formation

$$H_2 + C_2H_4 \xrightarrow[\text{RhCl(PPh}_3)_3]{} C_2H_6 \qquad (3)$$
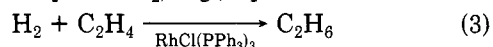
of $Rh(H)_2(Cl)(PPh_3)_3$. Similarly, an important step in the H–D exchange in alkanes[3] is the oxidative addition of C–H bonds; e.g., eq 4 may involve formation of $Pt(H)(CH_3)$-

$$CH_4 + D_2O \xrightarrow[\text{K}_2\text{PtCl}_4]{} CH_3D + HOD \qquad (4)$$
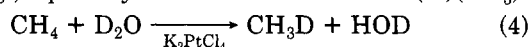
$(Cl)_4{}^{2-}$. In addition, reductive coupling to form C–C bonds is an important step in the cross coupling reaction catalyzed by Ni(II) and Pd(II);[4] e.g., eq 5 involves $Ni(Ar)(R)L_2$ → $NiL_2$ + Ar–R.

$$Ar-Cl + RMgCl \xrightarrow[\text{NiCl}_2\text{L}_2]{} Ar-R + MgCl_2 \qquad (5)$$
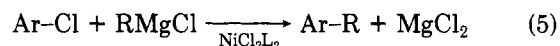
Because of the central role of oxidative addition/reductive elimination in organometallic chemistry, a number of recent experimental studies have been directed toward elucidating the details of such reactions. However, a

---

(1) Collman, J. P.; Hegedus, L. S. "Principles and Applications of Organotransition Metal Chemistry"; University Science Books: Mill Valley, CA, 1980.
(2) (a) James, B. R. "Homogeneous Hydrogenation"; Wiley: New York, 1973. (b) James, B. R. Adv. Organomet. Chem. 1979, 17, 319–405. (c) Brothers, P. J. Prog. Inorg. Chem. 1981, 28, 1–61.
(3) (a) Parshall, G. W. Catal. (London) 1977, 1, 335–368; (b) Shilov, A. E.; Shteinman, A. A. Coord. Chem. Rev. 1977, 24, 97–143. (c) Webster, D. E. Adv. Organomet. Chem. 1977, 15, 147–188.
(4) (a) Tamao, K.; Sumitani, K.; Kiso, Y.; Zembayashi, M.; Fujioka, A.; Kodama, S.; Nakajima, I.; Minato, A.; Kumada, M. Bull. Chem. Soc. Jpn. 1976, 49, 1958. (b) Negishi, E. "Aspects of Mechanism and Organometallic Chemistry"; Brewster, J. H., Ed.; Plenum Press: New York, 1978. (c) Kumado, M. Pure Appl. Chem. 1980, 52, 669–679. (d) Negishi, E. Acc. Chem. Res. 1982, 15, 340–348.

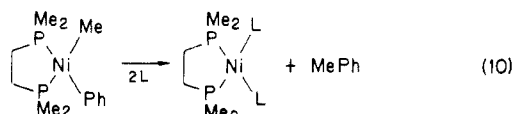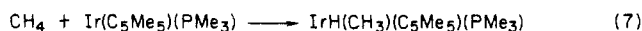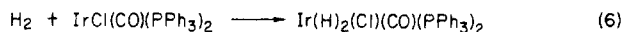number of puzzles remain, and there is yet no unified theoretical framework for understanding such processes for H–H, H–C, and C–C systems. The purpose of this paper is to add toward building this framework.

Current experimental evidence relating to these reactions is as follows.

**A. Experimental Evidence for Mechanism.** Mechanistic studies have been carried out on activation of $H_2$ by Ir(I) complexes (eq 6),[5] C–H activation by Ir(I)[6] and Rh(I)[7] complexes (eq 7), reductive coupling of C–H bonds from Pt(II) hydrido methyl complexes (eq 8),[8] and reductive coupling of C–C bonds from Pd(II)[9] (eq 9) and Ni(II)[10] complexes (eq 10). In all cases there is good evidence that these H–H, C–H, and C–C coupling or activation processes are concerted. Some of the evidence is as follows.

$$H_2 + IrCl(CO)(PPh_3)_2 \longrightarrow Ir(H)_2(Cl)(CO)(PPh_3)_2 \quad (6)$$

$$CH_4 + Ir(C_5Me_5)(PMe_3) \longrightarrow IrH(CH_3)(C_5Me_5)(PMe_3) \quad (7)$$

$$PtH(CH_3)(PPh_3)_2 \longrightarrow Pt(PPh_3)_2 + CH_4 \quad (8)$$

$$Pd(CH_3)_2(PPh_3)_2 \longrightarrow Pd(PPh_3)_2 + C_2H_6 \quad (9)$$



The activation of $H_2$ by Ir(I) complexes, (6), is believed to be concerted because (i) the oxidative addition of $H_2$ to Ir(I) complexes almost always yields a cis product,[5,11] (ii) the kinetics of the addition reaction are first order in both $H_2$ and the Ir(I) complex,[5a,b,d] and (iii) the entropy of activation $\Delta S^* \approx -23 \pm 3$ eu for oxidative addition of $H_2$ is very close to the entropy of reaction, $\Delta S \approx -28 \pm 3$ eu (which is dominated by the loss of the translational and rotational entropy of the $H_2$ molecule).[5b]

Activation of C–H bonds by Ir(I) complexes, (7), has been observed by a number of different research groups.[6] Janowics and Bergman[6c] conducted crossover experiments and measured the relative rates of insertion in different types of C–H bonds. Their results appear to be most consistent with a concerted process.

The mechanism of reductive elimination from Pt(II) hydrido alkyls, (8), has been studied by two research groups.[8] Abis, Sen, and Halpern[8a] used isotope labeling experiments to follow the decomposition of various Pt-(H)(Me)$L_2$ complexes and found that reductive elimination is intramolecular. Michelin et al.[8b] studied the decomposition of cis-Pt(H)(CH$_2$CF$_3$)(PPh$_3$)$_2$ [which decomposes at a slower rate than the hydrido methyl Pt(II) complexes] and found that (i) the rate of decomposition is first order in the reactant and (ii) the reaction has low values for the entropy of activation $\Delta S^*$ (2–8 eu). These results are consistent with a concerted unimolecular reductive elimination.

The mechanism of reductive elimination from Pd(II) dimethyl complexes, (9), has been studied by Stille et al.[9a-c] and by Ozawa et al.[9d] The lack of crossover products in the decomposition of Pd(CH$_3$)$_2$L$_2$ and Pd(CD$_3$)$_2$L$_2$ and the unimolecular kinetics observed in these experiments are consistent with a concerted process. Note, however, that the corresponding Pt complex will *not* reductively eliminate ethane (eq 11); it can, in fact, be sublimed before it will decompose.[12]

$$L_2Pt(CH_3)_2 \nrightarrow L_2Pt + C_2H_6 \quad (11)$$
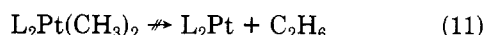
**B. Theoretical Strategy.** Four issues we wish to address here are as follows. (i) Are the processes always concerted? (ii) What are the relative barriers for H–H, H–C, and C–C coupling (and activation)? (iii) How does the nature of the metal affect the reaction? [Why is Pt(II) so different from Pd(II)?] (iv) What relation should there be between the processes for metal complexes vs. those for metal atoms? For reasons to be discussed below, we wanted to consider two related classes of systems where one class has exothermic reductive coupling for all three cases of $R_1$, $R_2$ = H, $CH_3$ and where the other class has exothermic oxidative addition for all three cases. Consequently, we examined reactions 12–17 where the first three

$$Pd(H)_2 \leftrightarrow Pd + H_2 \quad (12)$$

$$Pd(H)(CH_3) \leftrightarrow Pd + CH_4 \quad (13)$$

$$Pd(CH_3)_2 \leftrightarrow Pd + C_2H_6 \quad (14)$$

$$Pt(H)_2 \leftrightarrow Pt + H_2 \quad (15)$$

$$Pt(H)(CH_3) \leftrightarrow Pt + CH_4 \quad (16)$$

$$Pt(CH_3)_2 \leftrightarrow Pt + C_2H_6 \quad (17)$$

are exothermic (to the right) while the last three are endothermic. The Pd–H, Pd–CH$_3$, Pt–H, and Pt–CH$_3$ bonds in these systems should typify the M–H and M–C bonds of other organometallic complexes involving metals of comparable electronegativity and oxidation state.

From various previous studies,[13] we concluded that the reactions (eq 18) [where $R_1$, $R_2$ = H, $CH_3$ and M = Pt(0), Pd(0)] involve a change in the effective electronic configuration of M from an $s^1d^9$ configuration for $M(R_1)(R_2)L_2$ to a $d^{10}$ configuration for $ML_2$. Since the ground state of
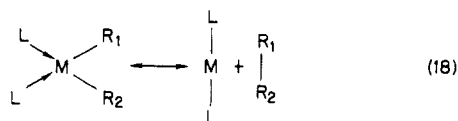


the Pd atom is $d^{10}$ (with the lowest $s^1d^9$ state lying 22 kcal/mol higher),[14] the Pd *atom* should be a fair model for

(5) (a) Chock, P. B.; Halpern, J. *J. Am. Chem. Soc.* **1966**, *88*, 3511–3514. (b) Vaska, L.; Werneke, M. F. *Trans. N.Y. Acad. Sci.* **1971**, *33*, 70–86. (c) Mays, M. J.; Simpson, R. N. F.; Stefanini, F. P. *J. Chem. Soc. A* **1970**, 3000–3002; (d) Hyde, E. M.; Shaw, B. L. *J. Chem. Soc., Dalton Trans.* **1975**, 765–767. (e) Longato, B.; Morandini, F.; Bresadola, S. *Inorg. Chem.* **1976**, *15*, 650–655. (f) Crabtree, R. H. *Acc. Chem. Res.* **1979**, *12*, 331–338. (g) Crabtree, R. H.; Quirk, J. M. *J. Organomet. Chem.* **1980**, *199*, 99–106. (h) Crabtree, R. H.; Hlatky, G. G. *Inorg. Chem.* **1980**, *19*, 571–572. (i) Crabtree, R. H.; Morehouse. S. M. *Ibid.* **1982**, *21*, 4210–4213. (j) Harrod, J. F.; Hamer, G.; Yorke, W. J. *J. Am. Chem. Soc.* **1979**, *101*, 3987–3989; (k) Harrod, J. F.; Yorke, W. J. *Inorg. Chem.* **1981**, *20*, 1156–1159. (l) Drouin, M.; Harrod, J. F. *Ibid.* **1983**, *22*, 999–1001.

(6) (a) Janowicz, A. H.; Bergman, R. G. *J. Am. Chem. Soc.* **1982**, *104*, 352–354. (b) Hoyano, J. K.; Graham, W. A. G. *Ibid.* **1982**, *104*, 3723–3725. (c) Janowicz, A. H.; Bergman, R. G. *Ibid.* **1983**, *105*, 3929–3939. (d) Wax, M. J.; Stryker, J. M.; Buchananan, J. M.; Kovac, C. A.; Bergman, R. G. *Ibid.* **1984**, *106*, 1121–1122. (e) Burk, M. J.; Crabtree, R. H.; Parnell, C. P.; Uriarte, R. J. *Organometallics* **1984**, *3*, 816–817.

(7) (a) Jones, W. D.; Feher, F. J. *J. Am. Chem. Soc.* **1984**, *106*, 1650–1663. (b) Periana, R. A.; Bergman, R. G. *Organometallics* **1984**, *3*, 508–510.

(8) (a) Abis, L.; Sen, A.; Halpern, J. *J. Am. Chem. Soc.* **1978**, *100*, 2915–2916. Halpern, J. *Acc. Chem. Res.* **1982**, *15*, 332–338. (b) Michelin, R. A.; Faglia, S.; Uguagliati, P. *Inorg. Chem.* **1983**, *22*, 1831–1834.

(9) (a) Gillie, A.; Stille, J. K. *J. Am. Chem. Soc.* **1980**, *102*, 4933–4941. (b) Loar, M. K.; Stille, J. K. *Ibid.* **1981**, *103*, 4174–4181. (c) Moravskiy, A.; Stille, J. K. *Ibid.* **1981**, *103*, 4182–4186. (d) Ozawa, F.; Ito, T.; Nakamura, Y.; Yamamoto, A. *Bull. Chem. Soc. Jpn.* **1981**, *54*, 1868–1880.

(10) Kohara, T.; Yamamota, T.; Yamamoto, A. *J. Organomet. Chem.* **1980**, *192*, 265–274.
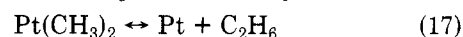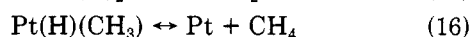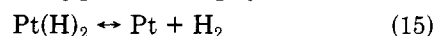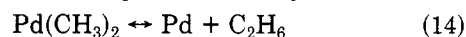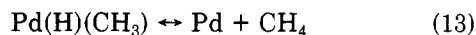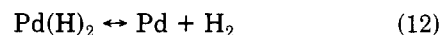
(11) Harrod et al. have observed a trans product from $H_2$ addition to Ir(I);[5j] however, this is believed not to be an initial product of the oxidative addition but rather the result of a rearrangement of one of the initial cis products.[5j]

(12) (a) Chatt, J.; Shaw, B. L. *J. Chem. Soc.* **1959**, 705–716. (b) Ruddick, J. D.; Shaw, B. L. *J. Chem. Soc.* **1969**, 2801–2808.

(13) Low, J. J.; Goddard III, W. A. *J. Am. Chem. Soc.* **1984**, *106*, 6928–6937.

(14) Moore, C. E. "Atomic Energy Levels"; NBS: Washington, D.C., 1971; Vol. III. (These state splittings were averaged over j states to cancel out spin–orbit coupling.)
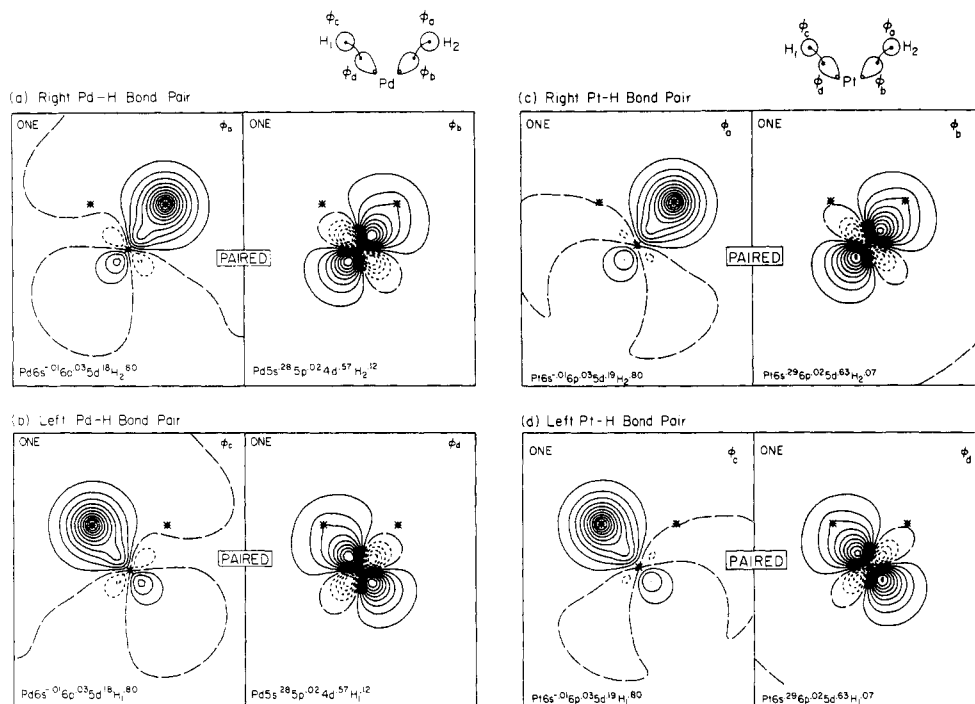
(a) Right Pd-H Bond Pair

(b) Left Pd-H Bond Pair

(c) Right Pt-H Bond Pair

(d) Left Pt-H Bond Pair

**Figure 1.** GVB orbitals for $PdH_2$ and $PtH_2$ [from GVB(2/4)-PP calculations]. Nuclei in the plane are indicated by asterisks. Positive contours are solid, negative contours are dotted, and nodal lines are long dashes. The spacing between contours is 0.05. Each GVB orbital is analyzed in terms of a Mulliken population.

Table I. Mulliken Populations for the GVB Bond Pairs of $M(R_1)(R_2)$[a]

| | system | | pop. of GVB orbitals | |
|---|---|---|---|---|
| M | $R_1$ | $R_2$ | M-H | M-CH$_3$ |
| Pd | H | H | $s^{0.28}p^{0.02}d^{0.57}H^{0.12}$ $(sp)^{0.02}d^{0.18}H^{0.80}$ | |
| Pd | H | CH$_3$ | $s^{0.3}p^{0.02}d^{0.43}C^{0.04}H^{0.19}$ $(sp)^{0.02}d^{0.15}C^{0.02}H^{0.81}$ | $s^{0.17}p^{0.01}d^{0.68}C^{0.12}$ $(sp)^{0.02}d^{0.17}C\,s^{0.10}p^{0.67}$ |
| Pd | CH$_3$ | CH$_3$ | | $s^{0.16}p^{0.03}d^{0.55}C^{0.24}$ $(sp)^{0.01}d^{0.20}C\,s^{0.28}p^{0.52}$ |
| Pt | H | H | $s^{0.29}p^{0.02}d^{0.63}H^{0.07}$ $(sp)^{0.02}d^{0.19}H^{0.80}$ | |
| Pt | H | CH$_3$ | $s^{0.30}p^{0.02}d^{0.60}H^{0.08}$ $(sp)^{0.01}d^{0.18}H^{0.80}$ | $s^{0.26}p^{0.01}d^{0.64}C^{0.09}$ $(sp)^{0.01}d^{0.16}C\,s^{0.12}p^{0.70}$ |
| Pt | CH$_3$ | CH$_3$ | | $s^{0.27}p^{0.01}d^{0.62}C^{0.10}$ $(sp)^{0.00}d^{0.15}C\,s^{0.14}p^{0.70}$ |

[a] For each bond there are two listings: the top one is the metal-like GVB orbital and the bottom one is the ligand-like orbital.

facile reductive elimination from various low-valent group VIII (8–10[55]) transition-metal complexes (eq 18). On the other hand, the ground state of the Pt atom is $s^1d^9$ (with the $d^{10}$ state lying 11 kcal/mol higher),[14] favoring oxidative addition and making the Pt atom a good model for facile oxidative addition processes.

The theoretical results for reactions 12–17 are described in section II, compared with experiment in section III, and compared with other theoretical work in section IV and Appendix A. Calculational details are described in section V.

## II. Summary of Results

**A. Electronic Promotion vs. Charge Transfer.** A major conclusion from these studies is that *oxidative addition requires promotion of the metal from the $d^{10}$ atomic configuration to the $s^1d^9$ configuration.* We find for R = H and $CH_3$ that the M-R bonds are covalent for both M = Pd and Pt, with each bond involving one electron in an orbital on R and one electron in an sd hybrid orbital on the metal. The $d^{10}$ configuration cannot make covalent bonds since all five d orbitals are doubly occupied; however, the $s^1d^9$ configuration with two singly occupied or-

bitals can mix these two orbitals to form two sd hybrids capable of forming covalent bonds to the two ligands. Thus *the metal atom is not oxidized* during the oxidative addition of $H_2$, $CH_4$, and $C_2H_6$ to Pd and Pt. Rather, the metal is promoted from the $d^{10}$ state incapable of forming covalent bonds to the $s^1d^9$ state capable of forming two covalent bonds.

Generalized valence bond (GVB) orbitals for the complexes studied in this work are shown in Figures 1, 2, and 3, with the hybridization of each orbital indicated just above the lower boundary of each orbital plot (these populations of GVB orbitals are summarized in Table I). In each case the ligand GVB orbital has 0.80 ± 0.03 electrons on the ligand with 0.17 ± 0.02 electrons on the Pt atom. For the Pt complexes, the metal GVB orbital has 0.08 ± 0.01 electrons on the ligand, 0.62 ± 0.02 electrons in a Pt d orbital, and 0.30 ± 0.02 electrons in Pt 6s and 6p orbitals (94% s and 5% p). Thus the metal orbitals are sd$^2$ hybrids. In the Pd complexes there is more variety in the character of the GVB orbital describing the metal part of the metal–carbon bond pair, with 0.24 electrons on the $CH_3$ for $Pd(CH_3)_2$, but 0.12 for $Pd(H)(CH_3)$. In addition, the sd hybrid character varies [from $s^1d^{1.7}$ for $PdH_2$
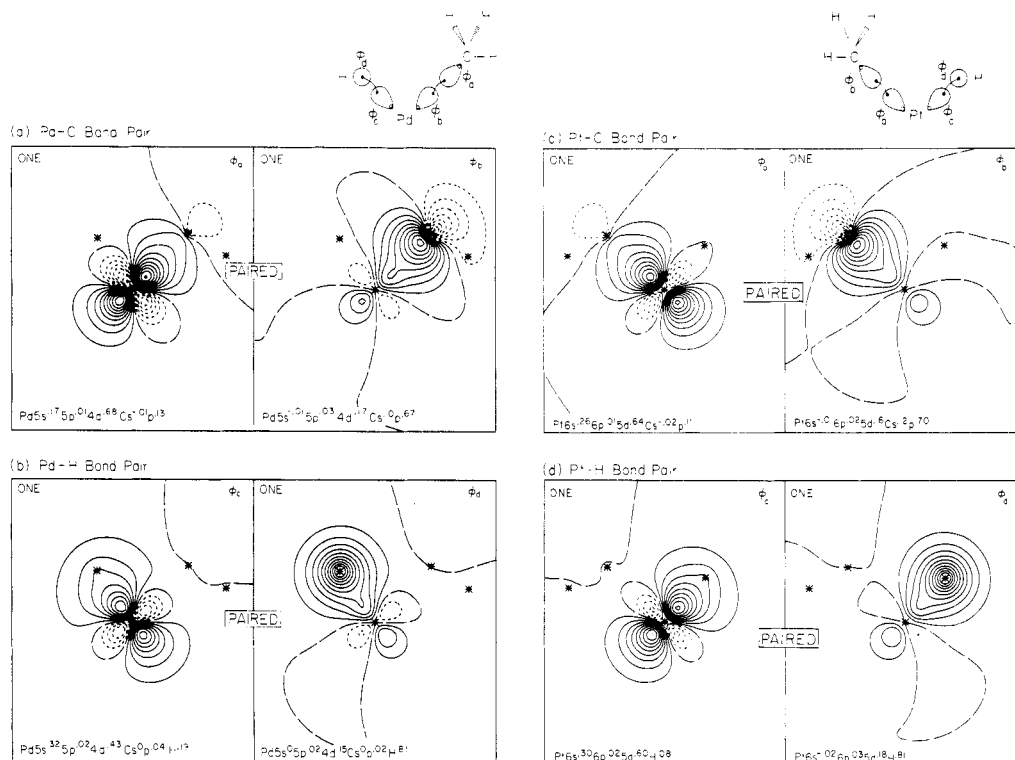
**Figure 2.** The GVB orbitals for $PdH(CH_3)$ and $PtH(CH_3)$ based on GVB(2/4) calculations.
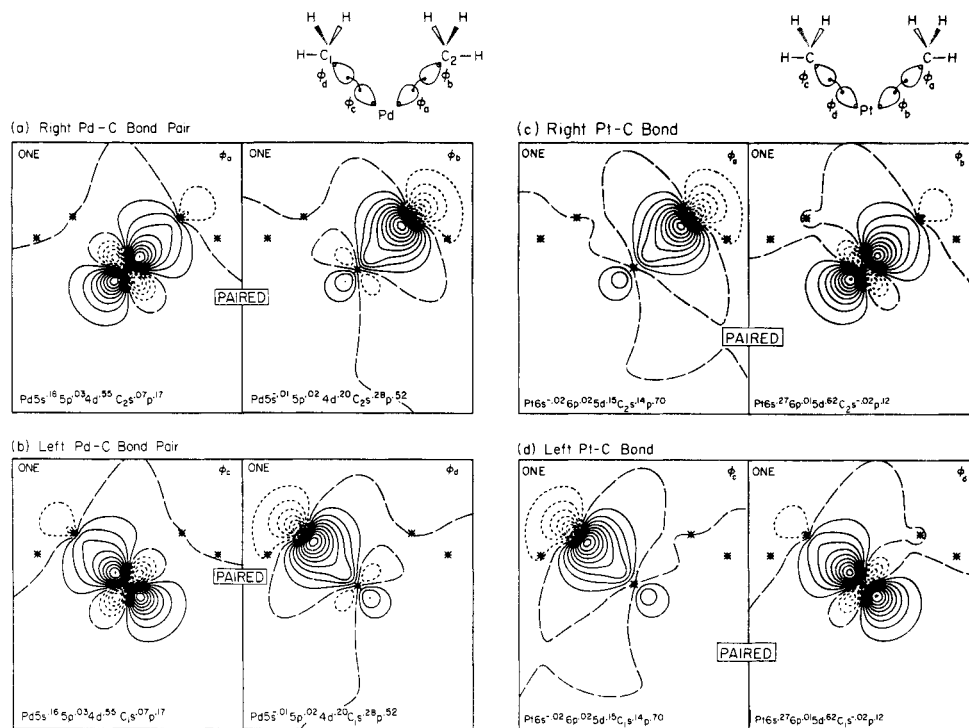


**Figure 3.** The GVB orbitals for $Pd(CH_3)_2$ and $Pt(CH_3)_2$ based on GVB(2/4) calculations.

to $s^1d^{1.3}$ for the Pd–H bond of $Pd(H)(CH_3)$ and from $s^1d^{3.8}$ for the Pd–C bond of $PdH(CH_3)$ to $s^1d^{2.9}$ for $Pd(CH_3)_2$]. We do not believe that these variations are as significant as the general result that the GVB orbitals for both Pt and Pd use sd hybrid orbitals to form bonds to H and $CH_3$ groups. These sd hybrids are similar in all cases, with somewhat more d than s character. The carbon atoms in methyl groups bonded to the metal are tetrahedral (within 1°) and $sp^3$ hybridized (see Appendix B). From total Mulliken populations (see Table II), the Pt complexes on the average have 9.03 d electrons and 1.06 s electrons, while Pd complexes have 9.23 d electrons and 0.69 s electrons

(a difference expected from the preference of Pd for d electrons).
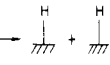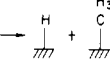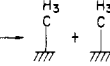
The fact that Pd–H, Pd–C, Pt–H, and Pt–C bonds are covalent is consistent with the Pauling electronegativities: Pd(2.2) and Pt(2.2) vs. H(2.1) and C(2.5).[15] Crabtree et al.[5f–i] have also suggested that the addition of $H_2$ to Ir(I) complexes is not oxidative based on observations that the oxidative addition of $H_2$ to cationic Ir(I) cyclooctadiene complexes is promoted by electron-withdrawing ligands

(15) Pauling, L. "The Nature of the Chemical Bond", 3rd ed.; Cornell University Press: Ithaca, NY, 1960; pp 88–98.

**Table II. Mulliken Total Populations for $M(R_1)(R_2)$**

| system | | | metal total pop. | | total pop. | | overlap of GVB bond orbitals | |
|---|---|---|---|---|---|---|---|---|
| M | $R_1$ | $R_2$ | M sp | M d | H | $CH_3$ | M-H | $M-CH_3$ |
| Pd | H | H | 0.76 | 9.36 | 0.94 | | 0.76 | |
| Pd | H | $CH_3$ | 0.71 | 9.19 | 1.05 | 9.06 | 0.76 | 0.68 |
| Pd | $CH_3$ | $CH_3$ | 0.60 | 9.15 | | 9.13 | | 0.72 |
| Pt | H | H | 1.16 | 9.15 | 0.85 | | 0.73 | |
| Pt | H | $CH_3$ | 1.05 | 9.03 | 0.89 | 9.04 | 0.74 | 0.71 |
| Pt | $CH_3$ | $CH_3$ | 0.97 | 8.91 | | 9.06 | | 0.71 |

**Table III. Summary of Energetics$^a$**

| reaction | | $\Delta E$ | $\Delta E^\dagger$ | zero-point energy$^b$ | | | $\Delta H°_{298} - \Delta H°_0$ | $\Delta H^\dagger_{298} - \Delta H^\dagger_0$ | $\Delta H°_{298}$ | $\Delta H^\dagger_{298}$ |
|---|---|---|---|---|---|---|---|---|---|---|
| | | | | $MR_1$ | $(MR_2)^\dagger$ | $M + R_2$ | | | | |
| $Pd(H)_2 \longrightarrow Pd + H_2$ | (12) | -3.6 | 1.6 | 7.9 | 6.4 | 6.3 | 1.2 | 0.3 | -4.0 | 0.4 |
| $Pd(H)(CH_3) \longrightarrow Pd + CH_4$ | (13) | -20.1 | 10.4 | 28.4 | 27.2 | 30.1 | 1.2 | 0.3 | -17.2 | 9.5 |
| $Pd(CH_3)_2 \longrightarrow Pd + C_2H_6$ | (14) | -16.0 | 22.6 | 47.6 | 48.3 | 43.9 | 0.9 | 0.3 | -18.8 | 23.6 |
| $Pt(H)_2 \longrightarrow Pt + H_2$ | (15) | 33.6 | | 7.9 | | 6.3 | 1.2 | | 33.2 | |
| $Pt(H)(CH_3) \longrightarrow Pt + CH_4$ | (16) | 16.1 | 29.0 | 28.4 | 27.2 | 30.1 | 1.2 | 0.3 | 19.0 | 28.1 |
| $Pt(CH_3)_2 \longrightarrow Pt + C_2H_6$ | (17) | 18.3 | 53.5 | 47.6 | 48.3 | 43.9 | 0.9 | 0.3 | 15.5 | 54.5 |
| $H_2 \longrightarrow$ [H‑H structure] Pt | | (-20.9) | | 8.6 | | 6.3 | -2.1 | | -20.7 | |
| | Pd | (-15.4) | | 8.6 | | 6.3 | -2.1 | | -15.2 | |
| $CH_4 \longrightarrow$ [H‑CH₃ structure] Pt | | (-3.4) | | 27.3 | | 30.1 | -2.1 | | -8.3 | |
| | Pd | (1.1) | | 27.3 | | 30.1 | -2.1 | | -3.9 | |
| $C_2H_6 \longrightarrow$ [CH₃‑CH₃ structure] Pt | | (-5.6) | | 46.0 | | 43.9 | -1.8 | | -5.3 | |
| | Pd | (-0.7) | | 46.0 | | 43.9 | -1.8 | | -0.4 | |

$^a$ The symbol $\dagger$ indicates transition state for the reaction. The separate atomic state for Pt is the spin-allowed singlet ($d^{10}$). $^b$ We have assumed that methyl groups bonded to the metal atom have free rotation about the M-C bond.

**Table IV. Average M-R Bond Energies**

| M | R | adiabatic bond energy $\bar{D}_A$, kcal/mol | intrinsic bond energy $\bar{D}_I$,$^a$ kcal/mol |
|---|---|---|---|
| Pd | H | 50 | 60 |
| Pt | H | 69 | 62 |
| Pd | $CH_3$ | 36 | 45 |
| Pt | $CH_3$ | 53 | 47 |

$^a$ State splittings are those determined at the GVB-RCI level (see section V).

and inhibited by electron donors$^{5f}$ and that an upfield shift of the vinyl carbon resonance occurs in the $^{13}$C NMR of Ir(COD)$_2$$^+$ (COD = 1,5-cyclooctadiene) on addition of H$_2$.$^{5g}$

Summarizing, the *oxidative addition* of H$_2$, CH$_4$, and C$_2$H$_6$ to $d^{10}$ metal centers *should be thought of in terms of promoting an electron from a doubly occupied d orbital to an unoccupied s orbital* in order to accommodate the formation of two covalent bonds *rather than the transfer of one electron to each ligand.* For Pd and Pt this promotion corresponds to the electronic transition from $d^{10}$ to $s^1d^9$ instead of ionizing two electrons from $d^{10}$ M(0) to form a $d^8$ M(II).

**B. Reaction Energetics and Bond Energies. 1. Reaction Energetics.** Before discussing the details of the reactions, we will examine the overall energetics (see Figures 4 and 5). For Pd, H-H, H-C, and C-C coupling is *exothermic* (with $\Delta H_{298}$$^{16}$ of -4.0, -17.2, and -19.0 kcal/mol resulting from $\Delta E$'s of -3.6, -20.1, and -16.0 kcal/mol, respectively), while for Pt these processes are *endothermic* (with $\Delta H_{298}$ of 33.2, 19.0, and 15.5 kcal/mol resulting from $\Delta E$'s of 33.6, 16.1, and 18.3 kcal/mol, respectively; see Table III). (For Pt these energies are for

(16) The vibrational frequencies used to estimate the zero-point energies were taken from those calculated for Pt(H)$_2$(PH$_3$)$_2$ and PtH(CH$_3$)(PH$_3$)$_2$.$^{16a}$ (a) Obara, S.; Kitaura, K.; Morokuma, K. *J. Am. Chem. Soc.* **1984**, *106*, 7482-7492; (b) The C-Pt-C bend was calculated by using the angle bending force constant derived from the potential of reaction 14. This gave a frequency for the H$_3$C-Pt-CH$_3$ bend of 190 cm$^{-1}$.
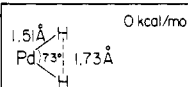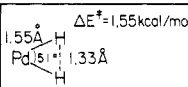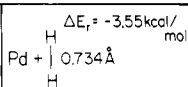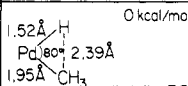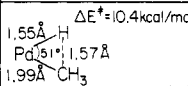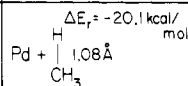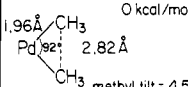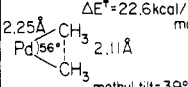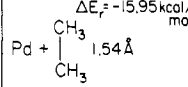
**Figure 4.** Summary of geometries and energetics for Pd + H$_2$ → PdH$_2$, Pd + CH$_4$ → PdH(CH$_3$), and Pd + C$_2$H$_6$ → Pd(CH$_3$)$_2$ based on GVB-RCI(4/8)×GVBCI(2/6) calculations.
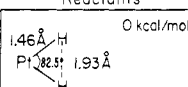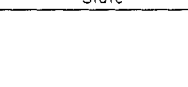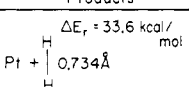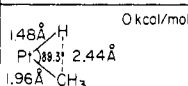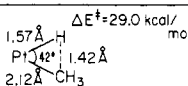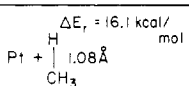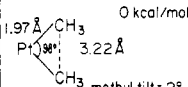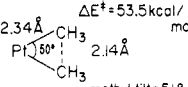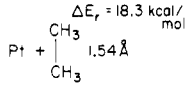


**Figure 5.** Summary of geometries and energetics for Pt + H$_2$ → PtH$_2$, Pt + CH$_4$ → PtH(CH$_3$), and Pt + C$_2$H$_6$ → Pt(CH$_3$)$_2$ based on GVB-RCI(4/8)×GVBCI(2/6) calculations.

the lowest spin-allowed process, leading to $d^{10}$ Pt atom.) These differences between Pd and Pt are easily understood on the basis of relative atomic excitation energies. Reductive coupling changes the metal from $s^1d^9$ to $d^{10}$, but for Pd the $s^1d^9$ state is 22 kcal/mol *higher* than $d^{10}$, while for Pt the $s^1d^9$ state is 11 kcal/mol *below* $d^{10}$. Thus, reductive coupling from Pd should be favored by 33 kcal/mol

(theoretical value 32 kcal/mol) over comparable reductive coupling from Pt. Indeed, we find the differences [$\Delta H_{298}$ for (2)] to be 37.2 kcal/mol for the dihydrides, 36.2 kcal/mol for hydrido methyl complexes, and 34.3 kcal/mol for the dimethyl complexes. Thus the GVB model of bonding allows one to use atomic excitation energies and the relative energetics of reductive coupling for one metal complex to estimate the energetics for other metals.

**2. Average Bond Energies.** For semiquantitative comparisons of various systems, it is often useful to have an idea of average bond energies for various types of bonds. There are two simple ways of doing this.

**Method 1: Adiabatic Bond Energies.** The adiabatic bond energy is defined as

$$\bar{D}_A(M-R) =$$
$$^{1/2}[\Delta H_{298}(MR_2 \rightarrow M + R_2) + \Delta H_{298}(R_2 \rightarrow 2R\cdot)]$$

The calculated reaction enthalpy for the reductive coupling is added to the $R_2$ bond energy[17] for a free $R_2$, and then the total is divided in half to give the adiabatic bond energy. This leads to $\bar{D}_A(Pt-H) = 69$ kcal/mol, $\bar{D}_A(Pt-C)$ = 53 kcal/mol, $\bar{D}_A(Pd-H) = 50$ kcal/mol, and $\bar{D}_A(Pd-C)$ = 36 kcal/mol. As a check on the consistency of average bond energies, we can use the bond energies calculated from the $\Delta H_{298}$ of reactions 12, 14, 15, and 17 to predict $\Delta H_{298}$ for reactions 13 and 16. This yields predicted values of $\Delta H_{298}$ of -19 kcal/mol for reaction 13 and 17 kcal/mol for reaction 16, which are both 2 kcal/mol lower than the calculated values of -17.2 and 19.0 kcal/mol. Overall, the Pd-R bonds are 19 and 17 kcal/mol weaker than the corresponding Pt-R bonds, which just represents the preference of Pd for $d^{10}$ over $s^1d^9$.

**Method 2: Intrinsic Bond Energies.** In order to eliminate the effect of $s^1d^9$-$d^{10}$ state splittings on the average bond energies, we define an intrinsic bond energy as

$$\bar{D}_I(M-R) = ^{1/2}[\Delta H_{298}(MR_2 \rightarrow M + R_2) +$$
$$\Delta H_{298}(R_2 \rightarrow 2R\cdot) + \Delta E(d^{10} \rightarrow s^1d^9)]$$

where the final state of the metal atom is taken as the $s^1d^9$ state. This is the intrinsic bond strength where the electronic state of the atom is not allowed to relax to a $d^{10}$ state. In this case, we obtain very similar bond energies for Pd and Pt, with $\bar{D}_I(Pd-H) = 60$ kcal/mol and $\bar{D}_I(Pt-H)$ = 62 kcal/mol, while $\bar{D}_I(Pd-CH_3) = 45$ kcal/mol and $\bar{D}_I(Pt-CH_3) = 47$ kcal/mol (see Table IV). Thus, these intrinsic energies plus atomic excitation energies should be most useful in using results for one metal to predict results for another.

**3. Energetics on Metal Surfaces.** For metal surfaces, one might expect that metal-metal bonding would tend to keep the surface atoms for the Ni triad in $s^1d^9$ states. If so, then the $\bar{D}_I$ should provide a reasonable estimate for the bond energy at metal surfaces.[18] (Band calculations for Pd and Pt have been interpreted in terms of an average $s^{0.4}d^{9.6}$ configuration,[19] somewhat more d occupation than in our complexes.) The predicted results for are

(17) The $D_{298}$ used in these calculations are $D_{298}(H-H) = 104.2$ kcal/mol, $D_{298}(H-CH_3) = 105.1$ kcal/mol, and $D_{298}(H_3C-CH_3) = 90.4$ kcal/mol. These bond energies were derived from spectroscopic measurements of $H_2$[17a] and the reported $D_{298}$[17b] for $H_3C-CH_3$ and $H-CH_3$. (a) Huber, K. P.; Herzberg, G. "Constants of Diatomic Molecules"; Van Nostrand: New York, 1979. (b) McMillen, D. F.; Golden, D. M. *Annu. Rev. Phys. Chem.* **1982**, *33*, 493-352.

(18) The vibrational frequencies (550, 1230, and 1230 cm⁻¹) used to calculate the zero-point energy correction of chemisorbed H are those from the EELS spectra of H on Pt(111).[18a] The zero point energy correction for chemisorbed $CH_3$ is that calculated and estimated for $CH_3$ chemisorbed on Ni(001).[18b] (a) Baro, A. M.; Ibach, H.; Bruchmann, H. D. *Surf. Sci.* **1979**, *88*, 384-398. (b) Low, J. J. Ph.D. Thesis, California Institute of Technology, Pasadena, CA, 1985, Chapter 4.
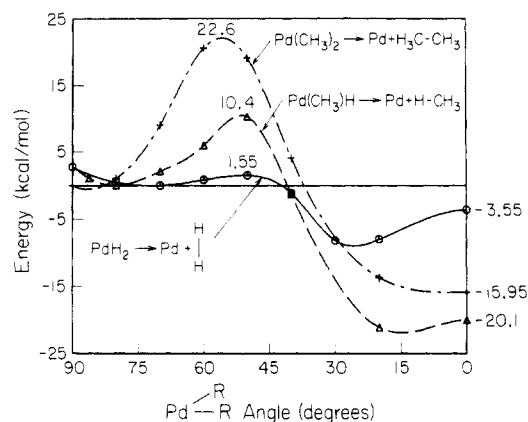


**Figure 6.** Potential curves for Pd + $H_2 \rightarrow PdH_2$, Pd + $CH_4 \rightarrow$ PdH(CH$_3$), and Pd + $C_2H_6 \rightarrow$ Pd(CH$_3$)$_2$ based on GVB-RCI-(4/8)×GVBCI(2/6) calculations.
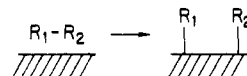


$$\Delta H_{298} =$$
-15 kcal/mol (Pd) and -20 kcal/mol (Pt) for $H_2$

$$\Delta H_{298} =$$
-4 kcal/mol (Pd) and -8 kcal/mol (Pt) for $H-CH_3$

$$\Delta H_{298} =$$
-10 kcal/mol (Pd) and -14 kcal/mol (Pt) for $H-C_2H_5$

$$\Delta H_{298} =$$
0 kcal/mol (Pd) and -5 kcal/mol (Pt) for $CH_3-CH_3$

The experimental heats of adsorption for $H_2$ on Pt and Pd surfaces are 20.8 kcal/mol[20] on Pd(111), 24.4 kcal/mol on Pd(110),[20] 9.5 kcal/mol on Pt(111),[21] and 12 kcal/mol on Pt[9(111) × (111)].[21] Thus our one-center Pd numbers predict surface Pd-H bonds about 3 kcal/mol weaker than experiment, whereas our numbers for Pt indicate surface Pt-H bonds about 5 kcal/mol stronger than observed.

Using the experimental results on $H_2$ to calibrate the predictions for the other reactions leads to

$$\Delta H =$$
-10 kcal/mol (Pd) and +1 kcal/mol (Pt) for $H-CH_3$

$$\Delta H =$$
-16 kcal/mol (Pd) and -6 kcal/mol (Pt) for $H-C_2H_5$

$$\Delta H =$$
-6 kcal/mol (Pd) and +4 kcal/mol (Pt) for $CH_3-CH_3$

As experimental data become available for such surface reactions, it will be interesting to see how energetics can be extrapolated between homogeneous and heterogeneous systems.

**4. Barriers for Reductive Coupling.** For the Pd-(R$_1$)(R$_2$) complexes, it is exothermic to reductively couple H-H, H-C, or C-C bonds; however, the barriers for these processes depend dramatically upon the nature of the ligands (see Figure 6):

$\Delta E^\ddagger_{H-H} = 1.6$ kcal/mol $\quad \Delta H^\ddagger_{298\ H-H} = 0.4$ kcal/mol

$\Delta E^\ddagger_{H-C} = 10.4$ kcal/mol $\quad \Delta H^\ddagger_{298\ H-C} = 9.5$ kcal/mol

$\Delta E^\ddagger_{C-C} = 22.6$ kcal/mol $\quad \Delta H^\ddagger_{298\ C-C} = 23.6$ kcal/mol

Similarly, for the corresponding Pt complexes (see Figure

(19) MacDonald, A. H.; Daams, J. M.; Vosko, S. H.; Koelling, D. D. *Phys. Rev. B: Condens. Matter* **1981**, *23*, 6377-6398.

(20) Conrad, H.; Ertl, G.; Latta, E. E. *Surf. Sci.* **1974**, *41*, 435-446.

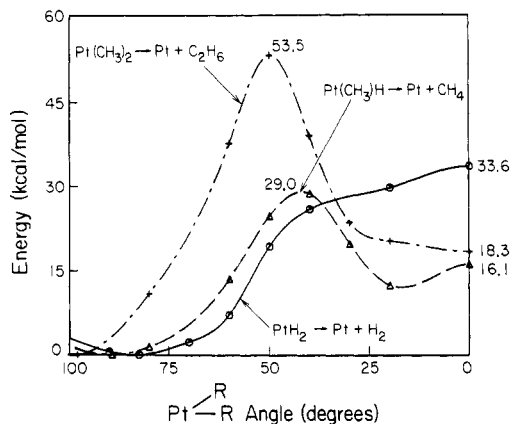(21) Weinberg, W. H. *Surv. Prog. Chem.* **1983**, *10*, 1-59.

**Figure 7.** Potential curves for Pt + $H_2 \rightarrow$ PtH$_2$, Pt + CH$_4 \rightarrow$ PtH(CH$_3$), and Pt + C$_2$H$_6 \rightarrow$ Pt(CH$_3$)$_2$ based on GVB-RCI(4/8)×GVBCI(2/6) GVB-RCI calculations.

7), the barriers for H–C and C–C coupling are far larger than the endothermicity.

$$E^{\ddagger}_{H-C} = 29.0 \text{ kcal/mol} \qquad H^{\ddagger}_{298\,H-C} = 28.1 \text{ kcal/mol}$$

$$E^{\ddagger}_{C-C} = 53.5 \text{ kcal/mol} \qquad H^{\ddagger}_{298\,C-C} = 54.5 \text{ kcal/mol}$$

Such dramatically different barriers would explain why Pt(H)(CH$_3$)(PH$_3$)$_2$ will reductively couple H–C bonds, whereas Pt(CH$_3$)$_2$(PH$_3$)$_2$ will *not* reductively couple C–C bonds. However, the question now is *why* the dramatic differences in barriers?

As discussed in more detail in section II.6, the reductive coupling process starts with a configuration having two covalent bonds involving sd hybrids on the metal



$$(19)$$
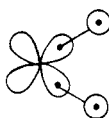
**s$^1$d$^9$ resonance configuration**

and converts this to a wave function with one covalent bond between the ligands and a doubly occupied d orbital on the metal



$$(20)$$
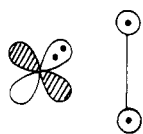
**d$^{10}$ resonance configuration**

At the transition-state geometry, both configurations must come into the wave function, wherein lies the difficulty. A hydrogen s orbital at the transition state is equally suited for either bonding configuration (19) or (20); however, for methyl, the bonding orbital is an sp$^3$ hybrid that can be directed *either* for making an M–C bond
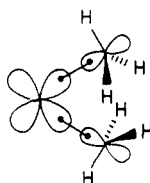


$$(21)$$

*or* for making a C–C bond
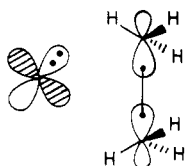


$$(22)$$
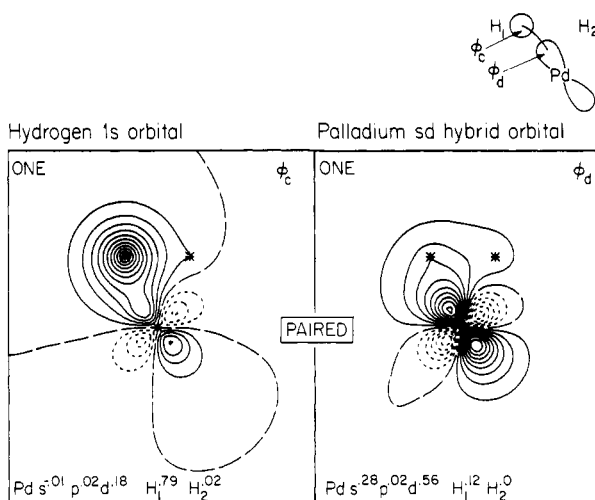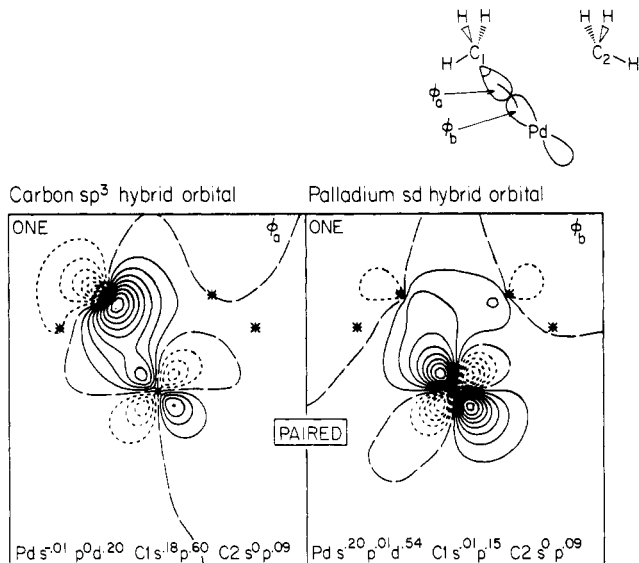


**Figure 8.** The GVB orbitals for PdH$_2$ and Pd(CH$_3$)$_2$ near the transition state for reductive elimination based on GVB(2/4)-PP calculations.

but *not* both. This is illustrated in Figures 8 and 9, which show the various orbitals for (12), (13), and (14) at a geometry near the saddle point. The CH$_3$ radical orients itself to a position intermediate between the geometries appropriate for (21) and for (22), leading to too weak a bond for either. The consequence of these effects is that each methyl group leads to a doubling of the barrier.

Clearly this methyl orientation effect can account for the observed differences in the efficacy of H–C vs. C–C coupling in Pt phosphine complexes. These results are consistent with the facile H–C coupling on Pt and C–C coupling on Pd, with the apparent lack of stability of the *cis*-Pd(H)(CH$_3$)(PH$_3$)$_2$ complex, and with the difficulty of C–C coupling from Pt dimethyl complexes.

**5. Geometries.** The bond distances for Pd–CH$_3$ and Pt–CH$_3$ bonds are nearly identical [1.96 ± 0.01 Å] for all complexes. For M–H bonds there is more variation with Pd–H = 1.51 ± 0.01 Å and Pt–H = 1.48 ± 0.01 Å. On the other hand, the bond angles for the various M(H)$_2$, M(H)(CH$_3$), and M(CH$_3$)$_2$ complexes vary considerably, being 73°, 80°, and 92° for Pd and 82°, 89°, and 98° for Pt.

The ideal bond angle between two bonds formed with symmetric linear combinations of a Pt s and a Pt d orbital is 90°. Thus, if the repulsive steric interactions were solely responsible for the trend of bond angle with methyl sub-

Table V. Mulliken Populations and Geometries along Reaction Path for Pd + $H_2 \rightarrow PdH_2{}^a$

| H–Pd–H angle, deg | Mulliken pop. | | | Pd–H dist, Å | H–H dist, Å |
|---|---|---|---|---|---|
| | Pt sp | Pt d | H | | |
| 90 | 0.80 | 9.28 | 0.958 | 1.51 | 2.14 |
| 80 | 0.79 | 9.31 | 0.949 | 1.51 | 1.94 |
| 70 | 0.76 | 9.36 | 0.940 | 1.51 | 1.73 |
| 60 | 0.71 | 9.41 | 0.939 | 1.52 | 1.52 |
| 50 | 0.62 | 9.49 | 0.948 | 1.55 | 1.31 |
| 40 | 0.50 | 9.59 | 0.957 | 1.60 | 1.10 |
| 30 | 0.36 | 9.71 | 0.963 | 1.71 | 0.89 |
| 20 | 0.14 | 9.88 | 0.989 | 2.12 | 0.74 |
| 0 | 0 | 10.0 | 1.00 | ∞ | 0.73 |

$^a$ The transition state is at a H–Pd–H angle of 51°.
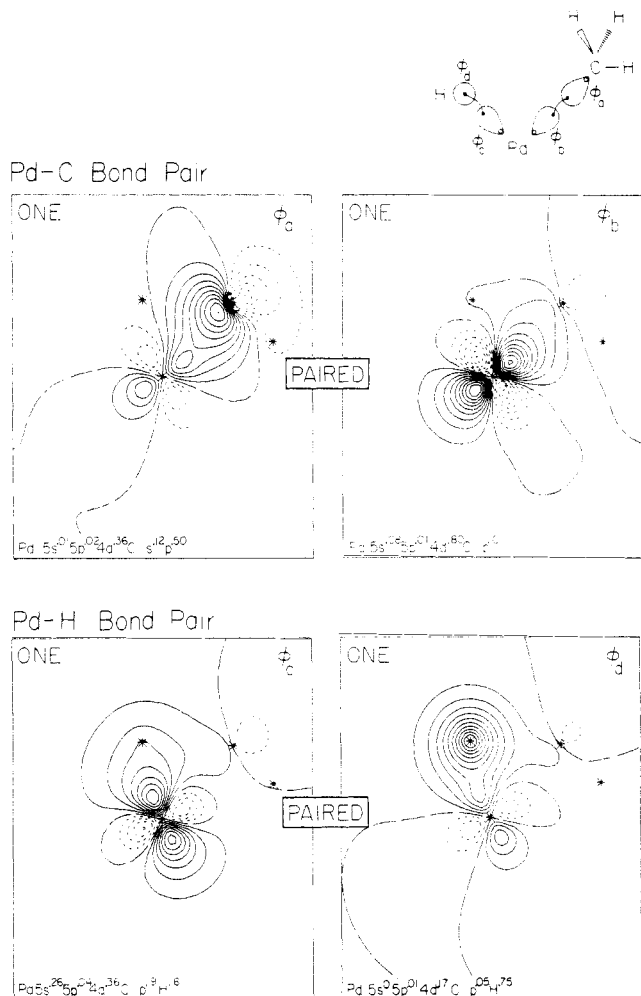


**Figure 9.** GVB orbitals for PdH(CH$_3$) near the transition state for reductive elimination based on GVB(2/4)-PP calculations.

stitution, one would expect to find R–M–R angles greater than 90°, but most of the equilibrium geometries have R–M–R angles less than 90°. Of course the actual hybridization is not exactly sd, and the calculated angles between the lobes of the metal-like GVB orbitals vary between 86° and 100° [86° for PtH$_2$, 91° for Pt(H)(CH$_3$), and 100° for Pt(CH$_3$)$_2$, leading to the an average of 92°] for Pt complexes and the average for Pd complexes is 88° ± 1°. The observed angles between the metal-like GVB orbitals for Pt track closely with the actual bond angle (80°, 91°, and 100° vs. 82°, 89°, and 98°, respectively); however, this does not constitute an explanation since we have not provided an a priori criterion for predicting the hybridization leading to these angles (other than being s$^{1.0}$d$^{1.0}$ to correspond to the s$^1$d$^9$ state). Thus, compared with the 90° expected from the s$^1$d$^9$ configuration, there must be attractive interactions between the ligands bound

to the metal atom. This attractive interaction can be explained by noting that the d$^{10}$ resonance structure has an R–R bonding interaction. The more important the d$^{10}$ resonance structure, the more attractive the interaction between ligands and the smaller the R–M–R angle. Since the d$^{10}$ resonance structure is more important in PdR$_2$ than in PtR$_2$, there will be greater bonding character between the R groups in PdR$_2$, providing a rationalization for the R–Pd–R bond angles being 10° smaller than the corresponding bond angles in the PtR$_2$ complexes (see Figures 4 and 5).

**6. Changes along Reaction Path.** As discussed above, there are two important resonance structures in the M-(R$_1$)(R$_2$) complexes responsible for determining the relative amounts of s and d character. The dominant resonance structure for PdR$_2$ and PtR$_2$ has the metal atom in an s$^1$d$^9$ configuration, shown schematically in (19) and denoted as the s$^1$d$^9$ resonance structure. Here the singly occupied s and d orbitals rehybridize to form sd hybrid orbitals that spin-pair (or form bonds) to the singly occupied orbitals of the R group. The second resonance structure, which dominates the wave function at the dissociated limit, has the metal atom in a d$^{10}$ configuration and an R–R bond, as shown schematically in (20). This is referred to as the d$^{10}$ resonance structure. As oxidative addition proceeds, the dominant resonance structure changes from the d$^{10}$ structure to the s$^1$d$^9$ structure. Since Pd prefers d$^{10}$ while Pt prefers s$^1$d$^9$, PdR$_2$ should have more of the d$^{10}$ resonance structure than PtR$_2$. This is consistent with the observation that PdR$_2$ complexes have larger d populations than PtR$_2$ complexes.

The Mulliken populations as a function of reaction coordinate for reaction 12 (see Table V) show that at the dissociated limit the Pd atom is in a d$^{10}$ state, and as the hydrogen molecule approaches, the Pd atom mixes in s$^1$d$^9$ character. Finally, when two Pd–H bonds have formed, the Pd atom has 75% s$^1$d$^9$ character (defined by the occupation of the Pd s orbital).

The spherically symmetric H$_{1s}$ orbital allows it to form bonds in more than one direction at a time. This multicentered bonding increases the H–H bonding character of the d$^{10}$ resonance structure, causes the H atoms to have an attractive interaction in the dihydrides, and leads to smaller H–M–H bond angles.

The sp$^3$ hybrid orbital of the CH$_3$ group is more directional than the H$_{1s}$ orbital. The shape of this orbital makes it difficult for this orbital to bond in more than one direction at a time. Consequently, there will be less bonding character in the d$^{10}$ resonance structure of the hydrido methyl complexes than in the dihydrides. This will cause the hydrido methyl complexes to have larger bond angles than the dihydrides.

Since the sp$^3$ orbitals of the methyl groups are directed at the metal, they have trouble forming the C–C bond in the d$^{10}$ structure. Consequently, the dimethyl complexes

have the least amount of bonding character in the $d^{10}$ resonance structure. Therefore, the dimethyl complexes should have the largest bond angles.

The increased ligand–ligand bonding in the $d^{10}$ resonance structure should stabilize it relative to the $s^1d^9$ resonance structure. This will cause metal d populations to be larger for dihydride complexes and smaller for the dimethyl complexes, which is consistent with the Mulliken populations in Table II.

The potential curves along the reaction paths are shown in Figures 6 and 7. In each of the potential curves the $R_1$–M–$R_2$ bond angle ($\theta_{R_1R_2}$) was fixed, and all other geometric parameters were fully optimized (see section V). In this manner, we were able to obtain the energy as a function of $\theta_{R_1R_2}$ from the $MR_2$ complex to the dissociated limit ($\theta_{R_1R_2} = 0°$).

The potential curves for reactions 12–14, 16, and 17 can be partitioned into three regions: 1. the $MR_2$ complex region, where the metal atom has $s^1d^9$ character and each R group forms a covalent bond to the metal; 2. the transition state region, where the M–R bonds are breaking and the R–R bond is forming (or vice versa), with a strong mixture of both the $d^{10}$ and $s^1d^9$ resonance structures; 3. the dissociated limit, where the R–R bond is fully formed and the metal is in the $d^{10}$ state.

In region 1 the M–R bond lengths change by less than 0.02 Å as the $\theta_{R_1R_2}$ is varied, indicating that the M–R bond is still intact. As the complex enters region 2, the M–R bonds begin to stretch and the methyl groups in the hydrido methyl and dimethyl complexes rotate so that their $sp^3$ orbitals are directed more toward the other R group.

At the transition state, the ligand–ligand bond distances are generally closer to the bound complex geometry than to the dissociated limit. Pd complexes have smaller distortions (they are more reactant-like) than the corresponding Pt complexes (see Figures 4 and 5) at the transition state, as would be expected from the Hammond postulate. The dimethyl complexes have the largest distortions. Pt + $H_2$ → $PtH_2$ differs from the other reactions studied here in that there is no barrier to oxidative addition (it is quite exothermic, 33.6 kcal/mol).

Past the transition state there exists a second minimum for the Pd + $H_2$, Pd + $CH_4$, and Pt + $CH_4$ cases. In this bound complex, the H–H or C–H bonds are intact and behave as Lewis bases, while the $d^{10}$ configuration of the transition metal serves as a Lewis acid (empty valence s orbital). The geometries for the Lewis acid/Lewis base complex are shown in Figure 10. These geometries were not separately optimized but were interpolated from the calculations along the reaction path. [Notice the lack of symmetry in the M($CH_4$) complexes.] As a result, the geometry obtained for each complex is not particularly accurate [the internal coordinates of $H_2$ and $CH_4$ in these complexes should be accurate, while the error in metal–ligand distance (±0.2 Å) and in orientation (±10°) will be larger]. However, Lewis acid/Lewis base complexes in these systems are clearly stable with respect to the dissociated limit. There seems to be a small increase in the H–H bond length (0.07 Å) and very little distortion in the C–H bond lengths of methane (two CH bonds of methane interact with the metal atom in this region). Our reaction path restricted the orientation of the methyl group in such a way that at most two C–H bonds could complex to the metal atom. Therefore, the Lewis acid/Lewis base complexes, with three C–H bonds complexed to the metal atom (probably the most stable), were not examined.

Previous calculations found a similar bound complex for $PdH_2$[22] and described it as a van der Waals complex. Since
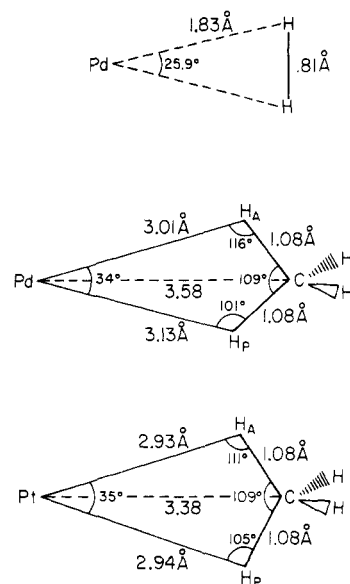


**Figure 10.** Geometries of Lewis acid/Lewis base complexes of Pd + $H_2$, Pd + $CH_4$, and Pt + $CH_4$. The bond energy with respect to dissociation is 5, 2, and 4 kcal/mol, respectively.

our wave function does not include the electronic configurations involved in the dynamic polarizations responsible for van der Waals forces (nor the f functions needed on the Pt for a proper description of such effects), our results cannot be explained in terms of a van der Waals complex.[23] Rather, they should be thought of as weak Lewis acid/Lewis base complexes. Similar $\eta^2$ bonding of $H_2$ to a transition metal has been observed experimentally in $M(CO)_3(PR_3)_2H_2$ (M = Mo, W; R = Cy, $i$-Pr) complexes studied by Kubas et al.[24a] and theoretically by Hay.[24b]

The interactions responsible for these Lewis base/Lewis acid complexes of $CH_4$ to metal atoms are probably identical with those involved in "agostic"[25a] interactions of C–H bonds and transition metals observed experimentally[25a] and theoretically[25b] in several complexes. This type of interaction has thus far only been observed for C–H bonds of ligands that are also covalently bound to the complex. The very small binding energies found in our calculations [5 kcal/mol for Pd($H_2$), 2 kcal/mol for Pd($CH_4$), and 4 kcal/mol for Pt($CH_4$)] are insufficient to balance the entropic contribution to the free energy of binding at room temperature ($\sim$10 kcal/mol), indicating that such bonds to alkyl groups that are not already part of the complex will in gas phase only be observed at low temperatures.

### III. Comparison with Experiment Comparison with Experiment

The results presented in the previous section explain many of the experimentally observed trends. Halpern et al.[8a] and Michelin et al.[8b] observed intramolecular reductive coupling from various hydridoalkylbis(phosphine)platinum(II) complexes. However, reductive coupling from Pt(II) dialkyls to form C–C bonds has never been reported,

(22) (a) Bagatur'yants, A.; Anikin, N.; Zhidomirov, G.; Kazanskii, V. *Zh. Fiz. Khim.* **1981**, *55*, 2035–2039. (b) Blomberg, M.; Brandemark, U.; Pettersson, L.; Siegbahn, P. *Int. J. Quantum Chem.* **1983**, *23*, 855–863.

(23) Brandemark, U. B.; Blomberg, M. R. A.; Pettersson, L. G. M.; Siegbahn, P. E. M. *J. Phys. Chem.* **1984**, *88*, 4617–4621. In this paper, convincing proof is provided that the Pd($H_2$) complex is not a van der Waals complex.

(24) (a) Kubas, R.; Ryan, R.; Swanson, B.; Vergamini, P.; Wasserman, H. *J. Am. Chem. Soc.* **1984**, *106*, 451–452. (b) Hay, P. J. *Chem. Phys. Lett.* **1984**, *103*, 466–469.

(25) (a) Brookhart, M.; Green, M. L. H. *J. Organomet. Chem.* **1983**, *250*, 395–408 and references therein. (b) Koga, N.; Obara, S.; Morokuma, K. *J. Am. Chem. Soc.* **1984**, *106*, 4625–4626.

even though this reaction is thought to be thermodynamically favored.[26] Rather, the Pt(II) dialkyls prefer β-hydride elimination[27] (eq 23 and 24), despite the fact that

$$\left[ (PR_3)_2Pt\begin{array}{c} H \\ \diagdown \\ CH_2-CH_3 \end{array} + H_2C{=}CH_2 \right] \rightarrow (PR_3)_2Pt + C_2H_6 + C_2H_4 \tag{23}$$

$$(PR_3)_2Pt\begin{array}{c} CH_2-CH_3 \\ \diagup \\ \diagdown \\ CH_2-CH_3 \end{array} \xrightarrow{\quad\times\quad} (PR_3)_2Pt + CH_3{-}CH_2{-}CH_2{-}CH_3 \tag{24}$$
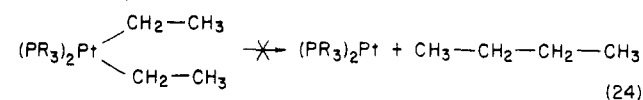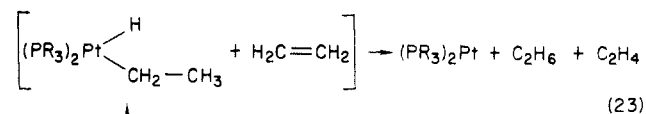
(24) is favored thermodynamically (by $\Delta H_{300}$ = -22.5 kcal/mol and $\Delta G_{300}$ = -11.0 kcal/mol).[28] These observations are consistent with our findings that C–H reductive coupling leads to a barrier half that for CC reductive coupling. This trend should be applicable to concerted addition/elimination reactions for other group VIII metals because it depends primarily on the relative shapes of H 1s and $CH_3$ sp$^3$ orbitals.

Unlike their Pt analogues, Pd(II) dimethyl complexes do reductively eliminate ethane, a result we attribute to the strong preference (by 34 kcal/mol relative to Pt) of Pd for the d$^{10}$ configuration, which leads to a greatly reduced barrier [we estimate 10 kcal/mol for $Pd(CH_3)_2(Ph_3)_2$ compared with 40 kcal/mol for $Pt(CH_3)_2(PH_3)_2$].[29] This is in agreement with observed reductive elimination of ethane from $Pd(CH_3)_2L_2$ complexes[9a,d] (where L = PPh$_3$, PPh$_2$CH$_3$; L$_2$ = PPh$_2$PCH$_2$CH$_2$PPh$_2$), and the fact that hydrogen will not oxidatively add to a Pd bis(phosphine) complex but does add to the corresponding Pt complex.[30]

Oxidative addition of $H_2$ to square-planar Ir(I) complexes is the most thoroughly studied system experimentally, and it is believed to involve a concerted mechanism.[5] In contrast to the results presented here for the addition of $H_2$ to Pt and Pd and earlier work for $H_2$ addition to Pt(PH$_3$)$_2$, the Ir(I) complexes have a relatively high barrier to oxidative addition (10–12 kcal/mol for Vaska's complex[5a,b,d]) and reductive elimination (25 kcal/mol). This difference probably arises from the difference in electronic configurations, with Pt and Pd having a spherically symmetric d$^{10}$ shell of electrons on the metal atom, while Ir(I) leads to square-planar four-coordinate complexes. Thus Pt(PH$_3$)$_2$[13] has a P–Pt–P angle of 180°, being determined by steric interactions between phosphines. Promoting the Pt(PH$_3$)$_2$ complex to a triplet state leads to a P–Pt–P bond angle of 100°, where the phosphine lone pairs maximize their overlap with the singly occupied $d_{yz}$ orbital of the triplet state.[13] On the other hand, Ir(I) has a strong preference for square-planar geometries. Addition of $H_2$ to such complexes should lead to a distortion of ligands

toward the six-coordinate Ir(III) product.[5b] Here a significant distortion away from square planar is required at the transition state in order to allow the d$^2$ → s$^1$d$^1$ excitation required for formation of the new Ir–ligand covalent bonds. Thus the higher barrier in Ir(I) is attributed to the lack of a symmetric d$^{10}$ shell and the concomitant strong preference for square planar geometries. Indeed, Vaska and Werneke[5b] proposed a similar effect, the "reorganization or rehybridization energy", whose magnitude was deduced from the trends observed in $\Delta H^{\ddagger}$ and $\Delta H$ for oxidative addition of $H_2$ to Ir(I) complexes. They equated this reorganization energy to the $\Delta H^{\ddagger}$ for reductive elimination of $H_2$. We find low barriers for concerted reactions of $H_2$ with Pd, Pt($^1$S), and Pt(PH$_3$)$_2$; therefore, the reorganization energy must be very small (~2 kcal/mol) for these d$^{10}$ systems.

It has generally been believed that oxidative addition (being oxidative) should be promoted by electron-rich metals.[6c] However, C–H activation of C–H bonds has been observed to occur for both electron-rich[6a-d] and electrophilic Ir systems.[6e] Since the electronegativity[14] of Ir(2.2) is the same as for Pt(2.2) and Pd(2.2), we expect it to form covalent bonds to H and $CH_3$ so that the electron density on the metal should have little effect on the energetics for oxidative addition (as observed).

In every case where stable hydridoalkyl complexes have been formed by oxidative addition of M to sp$^3$ C–H bonds, a photochemically generated Cp*ML (L = CO or PMe$_3$; M = Ir[6a-d] or Rh[7]; Cp* = c-C$_5$Me$_5$) complex has been involved. The Cp* ligand can easily occupy three coordination sites of the octahedral complex for Ir(III) or Rh(III). However, Cp*$^-$ cannot occupy three coordination sites of a square-planar complex. Thus, the Cp*ML complexes are distorted significantly away from the square planar preferred by Ir(I) and Rh(I) and hence have smaller reorganization energy for oxidative addition than does Vaska's complex [they are much closer to the octahedral geometry favored by Ir(III) and Rh(III) complexes].[31-33] Therefore, these complexes will have lower activation barriers and greater driving forces favorable for oxidative addition. Constraining the geometry of the ligands appears to be a more important effect than the electron richness of the metal center. Similar analyses have also been given by Saillard and Hoffmann,[31] Sevin,[32] and Dedieu and Strich.[33]

We find that oxidative addition of $H_2$, $CH_4$, and $C_2H_6$ to the Pd atom is uphill energetically. These results suggest that the Pd atom is unreactive with respect to $H_2$, $CH_4$, and $C_2H_6$. This is consistent with the results of Klabunde and Tanaka,[34c] who found no reaction of Pd codeposited with $CH_4$ at 10 K. This lack of reactivity of Pd at low temperatures is due to the unreactive nature of the d$^{10}$ state of Pd and the large excitation energy (21.9 kcal/mol) needed to promote the Pd atom to the s$^1$d$^9$ configuration that can make two covalent bonds.

In fact, no transition metal in its ground state has been found to be reactive with $CH_4$ at low temperatures.[34] This can be easily explained despite the diverse nature of transition metal atoms. Every transition metal except Pd has either a singly or doubly occupied valence s orbital in its ground state. In reactions 12, 13, and 16, the empty s orbital gave rise to attractive Lewis acid/Lewis base

(26) Halpern, J. *Acc. Chem. Res.* **1982**, *15*, 238–244.

(27) (a) Whitesides, G. M.; Gaasch, J. F.; Stedronsky, E. R. *J. Am. Chem. Soc.* **1972**, *94*, 5258–5270. (b) McDermott, J. X.; White, J. F.; Whitesides, G. M. *Ibid.* **1976**, *98*, 6521–6528. (c) Young, G. B.; Whitesides, G. M. *Ibid.* **1978**, *100*, 5808–5815. (d) McCarthy, T. J.; Nuzzo, R. G.; Whitesides, G. M. *Ibid.* **1981**, *103*, 1676–1678. (e) McCarthy, T. J.; Nuzzo, R. G.; Whitesides, G. M. *Ibid.* **1981**, *103*, 3396–3403. (f) Nuzzo, R. G.; McCarthy, T. J.; Whitesides, G. M. *Ibid.* **1981**, *103*, 3404–3410. (g) Komiya, S.; Morimoto, Y.; Yamamoto, A.; Yamamoto, T. *Organometallics* **1982**, *1*, 1528–1536.

(28) Pt(Et)$_2$(PEt$_3$)$_2$ is known to decompose via β-hydride elimination to yield ethylene ($\Delta H_f^{\circ}{}_{300}$ = 12.5 kcal/mol, $S_{300}$ = 52.4 eu) and ethane ($\Delta H_f^{\circ}{}_{300}$ = -20.2 kcal/mol, $S_{300}$ = 54.9 eu) rather than by reductive elimination to give n-butane ($\Delta H_f^{\circ}{}_{300}$ = -30.2 kcal/mol, $S_{300}$ = 74.1 eu) even though n-propane is the thermodynamically favored product ($\Delta H_{300}$ = -22.5 kcal/mol, $\Delta S_{300}$ = -34.2 eu, $\Delta G_{300}$ = -11.0 kcal/mol for $C_2H_4$ + $C_2H_6 \rightarrow$ n-C$_4$H$_{10}$). The $\Delta H_f^{\circ}{}_{300}$ and $S^{\circ}{}_{300}$ were taken from: Benson, S. W. "Thermochemical Kinetics", 2nd ed.; Wiley: New York, 1976.

(29) Low, J.J. Ph.D. Thesis, California Institute of Technology, Pasadena, CA, 1985, Chapter 3.

(30) Yoshida, T.; Otsuka, S. *J. Am. Chem. Soc.* **1977**, *99*, 2134–2140.

(31) Saillard, J.; Hoffmann, R. *J. Am. Chem. Soc.* **1984**, *106*, 2006–2028.

(32) Sevin, A. *Nouv. J. Chim.* **1981**, *5*, 233–241.

(33) Dedieu, A.; Strich, A. *Inorg. Chem.* **1979**, *10*, 2940–2943.

(34) (a) Billups, W. E.; Kararski, M. M.; Hauge, R. H.; Margrave, J. L. *J. Am. Chem. Soc.* **1982**, *102*, 7394–7396. (b) Ozin, G. A.; McCaffrey, J. G. *Ibid.* **1982**, *104*, 7351–7352. (c) Klabunde, K. J.; Tanaka, Y. *Ibid.* **1983**, *105*, 3544–3546.

interactions at long M-R distances, resulting in an decreased barrier for oxidative addition. For a metal where the s orbital is occupied, this orbital must become orthogonal to the incoming R-R bond, leading to a repulsive interaction at long $M-R_2$ distances. Thus, one would expect every transition metal in its ground state to have an activation barrier to oxidative addition.

For excited states of transition-metal atoms, one can have states in which the s orbital is unoccupied and for which oxidative addition is exothermic. For example, we find that Pt $(^1S) + H_2 \rightarrow PtH_2$ $(^1A_1)$ leads to no barrier. These predictions are consistent with experiments[34] that find photoexcited metal atoms reactive with methane at low temperatures. [Extended Hückel calculations of Sevin and Chaquin[35] lead to similar results.]

## IV. Comparison with Other Theoretical Work

Several previous theoretical studies[22b,23,36,37] have addressed various issues relevant to the oxidative addition/reductive elimination of $H_2$, $CH_4$, and $C_2H_6$ to transition-metal complexes, although most have not examined the full reaction surfaces. Using fixed bond distances, Tatsumi et al.[36a] calculated activation energies at the extended Hückel level for reductive elimination of $C_2H_6$ from $Pd(CH_3)_2(PH_3)_2$ and $H_2$ from $(PdH_4)^{4-}$ models. They found higher barriers for reductive couplings for C-C bonds (39.1 kcal/mol) than for H-H bonds (4.6 kcal/mol) because of the weakening necessitated by the rocking motion[36a] of the methyl group.

Balacz et al.[36b] carried out muffin-tin Xα calculations at assumed geometries for various complexes and suggested, on the basis of the shapes of the molecular orbitals, that three-center bonding might be more important in the reductive elimination of $H_2$ from $H_2PtL_2$ than for $CH_4$ from $H(CH_3)PtL_2$ or for $C_2H_6$ from $(CH_3)_2PtL_2$. (They did not calculate barriers or geometries.)

Previous theoretical studies[22,23] of $Pd(H)_2$ did not find the local minimum corresponding to the Pd-H bonded complex. However, these calculations did *not* include relativistic effects and consequently the $s^1d^9$ $(^3D)$ state [important in the $Pd(H)_2$ complex] is 15 kcal/mol too high[38] relative to the $d^{10}$ state. Since our calculated barrier for reductive coupling is only 1.5 kcal/mol, it is not surprising that nonrelativistic calculations of this minimum do not find a Pd-H bonded complex.

Obara et al.[16a] have recently reported ab initio calculations on oxidative addition of $H_2$ and $CH_4$ to $Pt(PH_3)_2$. Their transition-state geometry for $H_2$ addition is in reasonable agreement with our previously published results on the same system.[13] The transition-state geometry for $CH_4$ addition calculated by Obara et al.[16a] (C-Pt-H angle = 36°, Pt-$CH_3$ distance = 2.27 Å, and Pt-H distance = 1.59 Å) is remarkably close to ours (C-Pt-H angle = 42°, Pt-$CH_3$ distance = 2.12 Å, and Pt-H distance = 1.57 Å), considering the lack of phosphines in our model. Their energetics, however, are difficult to compare with ours since the Pt effective core potential used by Obara et al.[39] is known to give Pt-H bonds that are far too strong.[40] [We

used the Hay[41] effective core potential which gives excellent bond energies and excitation energies.] The similarity of the transition states indicates that the $PH_3$ ligands do not significantly affect the reaction path for reductive coupling of C-H bonds. We would expect $PH_3$ ligands to lower the barrier for reductive elimination, since phosphines stabilize the $d^{10}$ configuration relative to $s^1d^9$ and increase the driving force for reductive elimination from $Pt(H)_2(PH_3)_2$,[13] $Pt(H)(CH_3)(PH_3)_2$,[29] $Pt(CH_3)_2(PH_3)_2$,[29] and $Pd(CH_3)_2(PH_3)_2$.[29]

No other ab initio theoretical studies on oxidative addition/reductive elimination to Pd and Pt atoms have been reported. However, Siegbahn and co-workers[22b,37b] calculated potential surfaces at the contracted CI level for reactions 25 and 26. They find, in contrast to our results,

$$Ni + CH_4 \leftrightarrow NiH(CH_3) \qquad (25)$$

$$Ni + C_2H_6 \leftrightarrow Ni(CH_3)_2 \qquad (26)$$
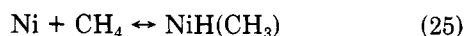
a higher barrier for C-H activation than for C-C activation. However, since these calculated activation barriers for H-C and C-C coupling are comparable to expected Ni-C bond energies, it is likely that that Siegbahn's calculations are modeling *nonconcerted* additions of Ni to $CH_4$ and $C_2H_6$.[37b] On the other hand, for our studies on Pd and Pt, a similar analysis leads to energies for forming radical intermediates far higher than our calculated barriers for the concerted processes. The sole exception is for C-C activation of Pt where the $\Delta H_{rad}$ is 43 kcal/mol, which is close to the $\Delta H^{\ddagger}$ for oxidative addition of 39 kcal/mol. This suggests that radical processes are competitive with concerted processes for reactions 17, 25, and 26 (Appendix B of the supplementary material reports a detailed analysis of $NiH_2$ where we test the reliability of the contracted CI's used in the Siegbahn study.[42])

For the organometallic systems being modeled in this paper, the metal atoms will generally have other ligands (e.g., phosphines) on them. We have shown[13] that the effect of phosphines is to stabilize the $d^{10}$ vs. $s^1d^9$ states in $Pt(PH_3)_2$ and expect the same effect for $Pd(PH_3)_2$ and $Ni(PH_3)_2$. The lowest *singlet* states of Pd and Pt are $d^{10}$, like the $M(PR_3)_2$ complexes that we are modeling, whereas the lowest singlet state of Ni is $s^1d^9$. Thus, the calculations for oxidative coupling of Pd and Pt atoms are more relevant for organometallic chemistry than similar calculations[37a,b] on Ni. Since the lowest singlet state of Ni differs so much from the lowest singlet state of Pd, Pt, and M-$(Pr_3)_2$(M = Ni, Pd, Pt), it is not surprising that Siegbahn's results are different from ours and run counter to the observed experimental trends.

## V. Calculational Details

**A. Potentials and Basis Sets.** We used ab initio effective core potentials (ECP) to represent the core electrons of Ni, Pd, and Pt. For Ni we used the ECP of Melius et al.,[43] with the five Gaussian d basis of Rappé et al.,[44] and the sp basis associated with the SHC potential

(35) Sevin, A.; Chaquin, P. *Nouv. J. Chim.* **1983**, *7*, 353-360.

(36) (a) Tatsumi, K.; Hoffmann, R.; Yamamoto, A.; Stille, J. K. *Bull. Chem. Soc. Jpn.* **1981**, *54*, 1857-1867. (b) Balazc, A. C.; Johnson, K. H.; Whitesides, G. M. *Inorg. Chem.* **1982**, *21*, 2162-2174.

(37) (a) Blomberg, M. R. A.; Siegbahn, P. E. M. *J. Chem. Phys.* **1983**, *78*, 986-987. (b) Blomberg, M. R. A.; Brandemark, U.; Siegbahn, P. E. M. *J. Am. Chem. Soc.* **1983**, *104*, 5557-5563. (c) Siegbahn, P. E. M.; Blomberg, M. R. A.; Bauschlicher, C. W. *J. Chem. Phys.* **1984**, *81*, 1373-1382.

(38) Martin, R. L.; Hay, P. J. *J. Chem. Phys.* **1981**, *75*, 4539-4545.

(39) Basch, H.; Topiol, S. *J. Chem. Phys.* **1979**, *71*, 802-814.

(40) Noell, J. O.; Hay, P. J. *J. Am. Chem. Soc.* **1982**, *104*, 4578-4584.

(41) Hay, P. J. *J. Am. Chem. Soc.* **1981**, *103*, 1390-1393.

(42) As part of examining the results from ref 37, we tested their use of contracted CI's in these calculations. The results are presented in Appendix B of the supplementary material. The contracted CI for $NiH_2$ leads to a bond angle for $NiH_2$ of 57°, whereas noncontracted CI's lead to results of 69°, indicating that the contracted CI is not adequate for bond angles where the energy curves are flat.

(43) Melius, C. F.; Olafson, B. D.; Goddard III, W. A. *Chem. Phys. Lett.* **1974**, *28*, 457-462.

(44) Rappé, A. K.; Smedley, T. A.; Goddard III, W. A. *J. Phys. Chem.* **1981**, *85*, 2607-2611.

**Table VI. Atomic State Splittings (kcal/mol) for Ni Triad**

| config | term | Ni exp[a] | Ni GVB-RCI[b] | Ni HF[c] | Pd exp[a] | Pd GVB-RCI[b] | Pd HF[c] | Pt exp[a] | Pt GVB-RCI[b] | Pt HF[c] |
|---|---|---|---|---|---|---|---|---|---|---|
| $s^1d^9$ | $^3D$ | 0.0 | 0.0 | 0.0 | 0.0 | 0.0 | 0.0 | 0.0 | 0.0 | 0.0 |
| $d^{10}$ | $^1S$ | 40.0 | 40.6 | 99.5 | -21.9 | -19.0 | 12.7 | 11.0 | 12.7 | 31.4 |
| $s^1d^9$ | $^1D$ | 7.7 | 7.9 | 18.4 | 11.4 | 11.2 | 13.8 | 32.1 | 25.9 | 27.0 |
| $s^2d^8$ | $^3F$ | 0.7 | 21.3 | -15.3 | 56.0 | 65.7 | 54.5 | 14.7 | 18.8 | 8.4 |

[a] Reference 14. [b] GVB-RCI(5/10) total energies in hartrees for the $^3D$ states of Ni, Pd, and Pt are -39.238987, -29.150011, and -27.551978, respectively. [c] Total energies in hartrees for the $^3D$ states of Ni, Pd, and Pt are -39.152853, -29.111329, and -27.506192, respectively, at the HF level.

of Rappé.[45] The relativistic effective core potentials (RECP) and basis of Hay[41] were used on Pd and Pt with a valence double-$\zeta$ basis. The Dunning[46] double-$\zeta$ contraction of the Huzinaga (9s5p) Gaussian basis was used on carbon. The active hydrogens bound directly to metal atoms were described by a triple-$\zeta$ contraction of the Huzinaga six Gaussian basis.[47] The nonactive methyl hydrogen atoms were described by a double-$\zeta$ contraction of the Huzinaga four Gaussian hydrogen basis scaled by a factor of 1.2.[46,47] For highly accurate bond energies and geometries, f functions should be included on the metal center, d functions on the C atoms, and p functions on the H atoms. However, the present basis is expected to be adequate for extracting the important issues about these various reactions.

## B. Configuration Interaction Calculations.

For $PdH_2$ and $PtH_2$ there are 12 valence electrons with four electrons involved in M-H bonds and eight involved in four pairs of metal d orbitals. As the $H_2$ molecule is eliminated, the four bonding electrons change dramatically, leading to two electrons describing H-H bonding and two describing a doubly occupied d orbital on the metal, while the other eight electrons change little. [Note that the spin-allowed product $M(H)_2 \rightarrow M + H_2$ involves a $d^{10}$ singlet state for both Pd and Pt.] Thus, to provide a balanced description of this system, we described each of the four fairly constant pairs of electrons in terms of a standard (one orbital per electron) GVB description. This is denoted as GVB(1/2) for each pair and GVB-PP(4/8) to indicate four pairs of electrons, each with two GVB orbitals for a total of eight. The PP (for perfect pairing) indicates that the spin coupling is that of a simple valence bond wave function with each of these four pairs singlet-spin paired. Expanded as a configuration interaction (CI) wave function in terms of natural orbitals, the GVB-PP-(4/8) wave function leads to $2^4 = 16$ configurations. Instead, we allowed the two electrons of each pair to recouple in all three possible ways using two orbitals, leading to a total of $3^4 = 81$ configurations, a calculation referred to as GVB-RCI(4/8). This GVB-RCI level of wave function allows the spin-coupling terms often important in transition metal systems and allows the interpair correlation so important for doubly occupied d orbitals.

The other four electrons have very different requirements for $Pd(H_2)$ vs. Pd + $H_2$. Thus, for $Pd(H)_2$, a standard GVB wave function leads to two localized orbitals for describing each Pd-H bond pair (as shown in Figure

**Table VII. Effect of Maximum Number of Open Shells and Level of Optimization on GVB-RCI(5/10) State Splittings in Pt Atom**

| state | state splittings, kcal/mol — six open shells — GVB-PP orbitals | six open shells — GVB-RCI orbitals | ten open shells GVB-RCI orbitals |
|---|---|---|---|
| $^3D(d^9s^1)$ | 0[a] | 0[b] | 0[c] |
| $^1S(d^{10})$ | 12.3 | 12.7 | 12.5 |
| $^1D(d^9s^1)$ | 26.1 | 25.9 | 25.9 |
| $^3F(d^8s^2)$ | 18.5 | 18.8 | 18.9 |

[a] Total energy in hartrees for the $^3D$ state of Pt is -27.551297 for GVB-RCI(5/10) with GVB-PP orbitals and restricted to six open shells. [b] Total energy in hartrees for the $^3D$ state of Pt is -27.551978 for GVB-RCI(5/10) with optimized orbitals and restricted to six open shells. [c] Total energy in hartrees for the $^3D$ state of Pt is -27.552461 for GVB-RCI(5/10) with optimized orbitals.

1). In terms of symmetry orbitals, this would lead to two $a_1$ and two $b_2$ orbitals. On the other hand, for separated $H_2$ and Pd, the standard GVB(2/4) description has two localized orbitals on the $H_2$ (leading to one $a_1$ and one $b_2$) and a correlated $d_{yz}$ orbital (leading to two $b_2$ orbitals). In order to provide an unbiased description of these reactions all along the reaction path, we used a wavefunction with three $a_1$ and three $b_2$ orbitals for the four bonding electrons. Allowing all possible occupations of the four electrons among these six orbitals leads to a wave function with 48 configurations and is referred to as GVB-CI(2/6). For all points along the reaction path we combined the GVB-RCI(4/8) and GVB-CI(2/6) wave functions to obtain a composite containing 8568 configurations[48] and denoted as GVB-RCI(4/8)×GVB-CI(2/6). The orbitals for this wave function were optimized for this 8568 configuration wave function using the GVB3 program.[49]

For calculations involving methyl groups, the inactive C-H bonds were uncorrelated [as in Hartree-Fock (HF)], and the M-C, active C-H, and C-C bonds were included in the GVB-CI space. All the other metal electrons were described in the same manner as $MH_2$.

A special virtue of this GVB approach to wave functions is that since the orbitals are divided into active (GVB-CI), semiactive (GVB-RCI), and inactive (HF) orbitals, the number of configurations does not increase when ligands are added, so large systems [e.g., $Pt(CH_3)_2(PH_2)_2$][29] can be treated nearly as easily as small ones.

Often it has been convenient to calculate the GVB-RCI wave function by using orbitals from corresponding GVB-PP calculations. This saves considerable time because the GVB-PP calculation does not require transformation of electron repulsion integrals to the molecular orbital basis. Indeed, such GVB-RCI calculations, using

(45) Rappé, A. K., unpublished results. We have tested the SHC basis sp basis by reoptimizing the H-Ni-H angle with the 5p basis associated with the one-electron MEP of Upton and Goddard [Upton, T. H.; Goddard III, W. A. "Chemistry and Physics of Solid Surfaces"; Vanselow, R.; England, W., Eds.; CRC Press: Boca Raton, 1982; Vol. 3, pp 127-162]. The MEP basis yielded an H-Ni-H angle of 83.2° at the GVB-CI(2/6) level, while the SHC gave 81.0° at the same level of calculation.

(46) Dunning, T. H., Jr.; Hay, P. J. In "Modern Theoretical Chemistry: Methods of Electronic Structure Theory"; Schaefer III, H. F., Ed.; Plenum Press: New York, 1977; Vol. 3, Chapter 1, pp 1-27.

(47) Huzinaga, S. *J. Chem. Phys.* **1965**, *42*, 1293-1302.

(48) This CI level was restricted to allow only six open shells. This was found to be an adequate level for the state splittings of Ni, Pd, and Pt atoms.

(49) Yaffe, L. G.; Goddard III, W. A. *Phys. Rev. A* **1976**, *13*, 1682-1691.

orbitals from GVB wave functions, yield atomic state splittings that are in good agreement with state splittings calculated self-consistently at the GVB-RCI level (see Table VI). However, it is necessary to optimize orbitals at the full GVB-RCI(4/8)×GVB-CI(2/6) level of wave function in order to self-consistently include the resonance between the $d^{10}$ and $s^1d^9$ configurations near the transition states for reactions 12–17.

To indicate how well this type of wave function does for atomic state splittings, we show in Table VII comparisons with experiment for HF and GVB-RCI(5/10)[13,50] state splittings. Here the GVB-RCI involves a total of ten optimized GVB orbitals for each state ($d^{10}$, $s^1d^9$, or $s^2d^8$), and we see that GVB-RCI does quite well, with errors of 1–3 kcal/mol in the $^1s(d^{10})$ to $^3D(s^1d^9)$ excitation and 0–6 kcal/mol in the energy of $^1D(s^1d^9)$ relative to $^3D(s^1d^9)$. These three states describe the dominant character of the wave function for the reactions studied in this paper. [Larger errors occur for the $s^2d^8$ state because angular correlation of the s pair of electrons, which is important for this state, was not included in this wave function. However, the $s^2d^8$ state is destabilized by addition of phosphine ligands, and it will not play a significant role[30] in the chemistry of such complexes.] In contrast, HF wave functions lead to errors of 20–60 kcal/mol in the $^1S(d^{10})$ to $^3D(s^1d^9)$ excitation and 2–11 kcal/mol in the position of $^1D(s^1d^9)$ relative to $^3D(s^1d^9)$.

Configurations with more than six singly occupied orbitals in the GVB-RCI wave function lead to numerous spin eigenfunctions (SEF) (e.g., a triplet with ten open shells has 90 SEF's). In order to save computer time, it is convenient to restrict the wave function so that there is a maximum of six open shells in any configuration. Thus the GVB-RCI for the $^1S$ state of Pt restricted to six open shells contains 72 configurations and 328 SEF's, whereas the full GVB-RCI contains 81 configurations with 642 SEF's. Table VI shows the differences in state splittings of Pt atom for calculations in which the number of open shells was restricted to a minimum of six compared with the case where no restrictions were made (up to ten open shells). The restriction of a maximum of six open shells leads to errors of only ~0.2 kcal/mol in the atomic state splitting relevant for this work, an error quite tolerable for our studies. We should emphasize that inclusion of at least six open shells is required in order to describe interpair correlations (a single excitation within one GVB pair times a single excitation within another GVB pair) for both the triplet and open-shell singlet states of the atom. In conclusion, the use of the six-open-shell restriction is justified for these studies, and all wave functions reported here are restricted to a maximum of six open shells unless otherwise noted.

**C. Geometry Optimization.** We used a distinguished coordinate method[51] to follow the potential curve from

---

(50) This level is very close to atomic wave functions at the dissociated limit of reactions 1–6.

(51) (a) Rothman, M. J.; Lohr, L. L. *Chem. Phys. Lett.* **1980**, *70*, 405. (b) Williams, I. H.; Maggiora, G. M. *THEOCHEM* **1982**, *89*, 365–378. Williams and Maggiora have shown that the distinguished coordinate method can yield a discontinuous reaction path if multiple local minima exist for the same value of distinguished coordinate. Since the M–H and M–CH₃ equilibrium bond lengths are much longer than the corresponding R–H and R–CH₃ bond lengths, it is not likely that more than one local minimum can exist for any value of R₁–M–R₂ bond angle in the bound complex to transition-state region. The M–R bond lengths in this region are close to those of the bound complex. If another minimum existed, it would have an R₁–R₂ distance closer to those of the products, which would force unphysically short M–R bond lengths. The typical symptom of a discontinuous reaction path would be a discontinuous change in geometric parameters, which is not evident in our results (see Appendix B).

**Table VIII. Effect of Electron Correlation on R₁-M-R₂ Equilibrium Bond Angles**

| | system | | bond angle, deg | | |
|---|---|---|---|---|---|
| M | R₁ | R₂ | HF | GVB-CI(2/6) | GVB-RGI-(4/8) × GVB-CI-(2/6) |
| Pd | H | H | 68 | 73 | 73 |
| Pt | H | H | 84 | 81 | 84 |
| Pd | H | CH₃ | 83 | 83 | 80 |
| Ni | H | H | 99[a] | 81[a] | 76[a] |

[a] Bond length frozen at geometry of Blomberg and Siegbahn.[37a]

reactants to products. Each geometry was calculated by holding the R–M–R angle fixed and optimizing all other geometric parameters for the HF wave function. With use of this sequence of geometries, we then carried out the self-consistent GVB-RCI(4/8)×GVB-CI(2/6) calculations. This allowed us to follow a continuous path from reactant to products for each system studied and to extract the concepts permitting us to explain the various features and to interpret the experiments. To obtain various critical points (minima and saddle points), we fitted the variations in energy and all other geometric parameters along the reaction path to cubic splines and interpolated the geometric parameters for the optimum energy. Thus, the geometries are not as accurate as they would be if separate energy optimizations had been carried out.

To determine the effect of electronic correlation on geometry, we calculated (see Table VIII) the equilibrium bond angles for PdH₂, PtH₂, PdH(CH₃), and NiH₂ at the HF, GVB-CI(2/6), and GVB-RCI(4/8)×GVB-CI(2/6) levels. For Pd and Pt complexes, the bond angle determined at the HF level is within 5° of the GVB-RCI(4/8)×GVB-CI(2/6) level.

In order to test the effects of correlation on the transition-state geometries, we reoptimized the geometry of PdH₂ at the GVB-RCI(4/8)×GVB-CI(2/6) level. This optimized transition state has a Pd–H distance of 1.595 Å and an H–Pd–H bond angle of 50.6°, with an activation energy of 0.74 kcal/mol (vs. 1.547 Å, 50.8°, and 1.551 kcal/mol for interpolated value based on the HF distinguished coordinate studies followed by GVB-RCI). These changes of 0.048 Å in Pd–H distance, 0.2° in bond angle, and 0.81 kcal/mol in activation barrier[52] indicate that use of the GVB calculations along the HF reaction path provides a reasonable description for these reactions.

Our calculations for reductive elimination of dimethyl and dihydride complexes assume a transition state with $C_{2v}$ symmetry. It is possible that the transition state for these reactions has lower symmetry.[53] However, it has been shown that the $C_{2v}$ transition state is a true saddle-point in recent ab initio calculations on a similar system, oxidative addition of H₂ to Pt(PH₃)₂.[16a,54] Therefore it is plausible that the $C_{2v}$ transition state for H–H coupling from PdH₂ and C–C coupling from Pd(CH₃)₂ is also a true

---

(52) A similar energy lowering would be expected for the PdH₂ complex if the geometry was reoptimized at the RCI(4/8)×GVB-CI(2/6) level.

(53) (a) Metiu, H.; Ross, J.; Silbey, R.; George, T. F. *J. Chem. Phys.* **1974**, *8*, 3200–3209. (b) Stanton, R. E.; McIver, J. W. *J. Am. Chem. Soc.* **1975**, *97*, 3632–3646. (c) Pechukas, P. *J. Chem. Phys.* **1976**, *64*, 1516–1521.

(54) Kitaura, K.; Obara, S.; Morokuma, K. *J. Am. Chem. Soc.* **1981**, *103*, 2891–2892.

(55) In this paper the periodic group notation in parentheses is in accord with recent actions by IUPAC and ACS nomenclature committees. A and B notation is eliminated because of wide confusion. Groups IA and IIA become groups 1 and 2. The d-transition elements comprise groups 3 through 12, and the p-block elements comprise groups 13 through 18. (Note that the former Roman number designation is preserved in the last digit of the new numbering: e.g., III→3 and 13.)

**Table IX. Effect of Correlation on Reaction Energetics and on Transition-State Geometry[a]**
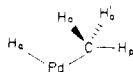
| | Hartree–Fock | | | GVB-CI(2/6) | | | RCI(4/8)×GVB-CI(2/6) | | |
|---|---|---|---|---|---|---|---|---|---|
| reaction | $\Delta E^\ddagger$ | R–M–R[‡] angle | $\Delta E$ | $\Delta E^\ddagger$ | R–M–R[‡] angle | $\Delta E$ | $\Delta E^\ddagger$ | R–M–R[‡] angle | $\Delta E$ |
| $Pd(H)_2 \rightarrow Pd + H_2$ | 0.3 | 55.8 | −17.6 | 4.3 | 44.5 | 0.4 | 1.6 | 50.6 | −3.6 |
| $Pd(H)(CH_3) \rightarrow Pd + CH_4$ | 7.2 | 53.3 | −36.5 | 14.9 | 49.7 | −16.3 | 10.4 | 51.3 | −20.1 |
| $Pd(CH_3)_2 \rightarrow Pd + C_2H_6$ | 27.5 | 59.0 | −33.0 | 30.9 | 56.5 | −13.8 | 22.6 | 55.8 | −16.0 |
| $Pt(H)_2 \rightarrow Pt + H_2$ | | | 26.2 | | | 33.8 | | | 33.6 |
| $Pt(H)(CH_3) \rightarrow Pt + CH_4$ | 26.1 | 44.3 | 3.7 | 36.3 | 40.5 | 21.2 | 29.0 | 42.1 | 16.1 |
| $Pt(CH_3)_2 \rightarrow Pt + C_2H_6$ | 42.8 | 52.0 | 5.1 | 69.3 | 49.8 | 21.7 | 53.1 | 49.8 | 18.3 |

[a] All angles in deg; all energies and kcal/mol. R–M–R[‡] denotes angle at transition state.

**Table X. Geometries and Energies Along Reaction Path for Pd + CH$_4$ → Pd(H)(CH$_3$)[a]**

| | | | | | | | | energy[b] | |
|---|---|---|---|---|---|---|---|---|---|
| geometric parameters[a] | | | | | | | HF | GVB-CI(2/6) | GVB-RCI-(4/8) × GVB-CI-(2/6) |
| H–Pd–C H$_3$ angle | Pd–H$_a$ dist | Pd–C dist | C–H$_a$ dist | H$_{Me}$–C–Pd angle[c] | H$_{Me}$–C–H$_a$ angle[c] | H$_p$–C–Pd angle | | | |
| 86 | 1.51 | 1.95 | 2.39 | 172.2 | 149 | 101.4 | 36.63 | 16.41 | 21.07 |
| 80 | 1.53 | 1.96 | 2.26 | 176.4 | 142 | 104.2 | 36.66 | 16.48 | 20.01 |
| 70 | 1.52 | 1.98 | 2.04 | 170.2 | 145 | 100.7 | 38.67 | 19.30 | 22.12 |
| 60 | 1.53 | 2.01 | 1.82 | 161.8 | 151 | 91.9 | 41.85 | 24.96 | 25.98 |
| 50 | 1.55 | 1.99 | 1.55 | 154.2 | 156 | 84.7 | 42.89 | 31.18 | 30.23 |
| 40 | 1.70 | 2.15 | 1.38 | 142.8 | 165 | 73.5 | 29.4 | 24.28 | 18.73 |
| 30 | 2.03 | 2.44 | 1.22 | 137.6 | 170 | 61.6 | 10.20 | 6.52 | 4.49 |
| 20 | 2.64 | 3.08 | 1.08 | 123.4 | 180 | 53.5 | 0.04 | −0.39 | −1.15 |
| 0 | ∞ | ∞ | 1.08 | | 180 | | 0 | 0 | 0 |

[a] All angles in deg; all distances in Å; all energies angle held kcal/mol. More complete information is given in Table II-A of the supplementary material. Each geometry optimized at the HF level with the H–Pd–CH$_3$ angle held fixed.

[b] Total energies in hartrees at the dissociated limit are −69.292 703 for HF, −69.317 023 for GVB-CI(2/6), and −69.387 700 for RCI(4/8)-*GVB-CI(2/6). [c] H$_{Me}$ is defined to be the center of mass of the methyl protons.

saddlepoint; however, we did not demonstrate this (by solving for the eigenvectors of the Hessian and showing there to be one negative eigenvalue).

**D. Details of Reaction Surface.** Table IX shows the effect of electron correlation on $\Delta E^\ddagger$, R–M–R angle at the transition state, and $\Delta E$. The trends in $\Delta E^\ddagger$ follow the same general trend as the $\Delta E$ for these reactions except with smaller magnitudes. The optimized geometries along the reaction path for the various reactions studied in this paper[(12)–(17)] have been collected into the supplementary material (Tables A-I to A-VI). Probably the most interesting is reaction 13 for which an abbreviated compilation is included in Table X. All of the geometries were optimized at the HF level (described in section V). We also report energies for HF, GVB-CI(2/6), and GVB-RCI(4/8)×GVB-CI(2/6) wave functions, all of which were found[13] to be consistent levels of calculation for the reaction H$_2$ + Pt(PH$_3$)$_2$ → H$_2$Pt(PH$_3$)$_2$.

The following trends can be extracted from these results. In going from HF to GVB-CI(2/6), oxidative addition always becomes *more* favorable (or reductive elimination is made less favorable). This occurs because the GVB-CI(2/6) wave function includes terms that provide a better description of the two M–R bonds, which have larger

correlation errors than the corresponding pairs for the dissociated limit (involving a metal d pair and an H–H bond pair). In going from the GVB-CI(2/6) level to the GVB-RCI(4/8)×GVB-CI(2/6) level, the additional terms describe correlation effects *between* d electrons. These terms are needed to get accurate d$^{10}$–s$^1$d$^9$ splittings and always stabilize the d$^{10}$ ($^1$S) state relative to the s$^1$d$^9$ ($^3$D) state. This makes oxidative addition *less* favorable (and reductive elimination more favorable). Thus there is some degree of cancellation in the correlation errors for HF.